December 2016

Seismic Analysis of Geosynthetic-reinforced Soil (GRS) Bridge Abutments with Modular Block Facing

Roonak Ghaderi
University of Wisconsin-Milwaukee

SEISMIC ANALYSIS OF GEOSYNTHETIC-REINFORCED SOIL (GRS) BRIDGE ABUTMENTS WITH MODULAR BLOCK FACING

by

Roonak Ghaderi

A Dissertation Submitted in
Partial Fulfillment of the
Requirements for the Degree of

Doctor of Philosophy
in Engineering

at

The University of Wisconsin-Milwaukee

December 2016

ABSTRACT

SEISMIC ANALYSIS OF GEOSYNTHETIC-REINFORCED SOIL (GRS) BRIDGE ABUTMENTS WITH MODULAR BLOCK FACING

by

Roonak Ghaderi

The University of Wisconsin-Milwaukee, 2016

Under the Supervision of Professor Sam Helwany

The response of Geosynthetic Reinforced Soil (GRS) bridge abutments to earthquake loading remains a concern despite their great success under static loads. In order to advance and implement this new technology, especially in seismically active regions, this study was undertaken to examine the performance of GRS bridge abutments under seismic loads in a rational and critical manner.

This research is focused on single span, simply supported bridges. The current seismic design methods, including pseudo-static and displacement methods, are not specifically developed for GRS bridge abutments where the foundation of the bridge superstructure is placed on the top surface of the GRS abutment and generally is subjected to large, sustained and often eccentric

loads. This study is aimed to predict the seismic behavior of GRS bridge abutments with modular block facing.

The full scale seismic GRS bridge abutment experiment was simulated using finite element program LS-DYNA.

A series of laboratory testing of the materials were carried out to obtain results which assisted in determining the material model parameters used to represent the behavior of the components of the GRS bridge abutment system in the finite element model. The lab experiments and the process of determining material parameters are presented in detail.

The results of the shake table test and finite element model were compared and a good agreement was found between experimental and finite element results. The validated finite element model was used to perform rigorous parametric analyses on the GRS abutments subjected to various earthquake loadings.

In the parametric analysis the influence of soil friction angle, geotextile stiffness, geotextile spacing and bridge height as design variables were investigated. The response of the model abutment including the maximum and permanent lateral displacement of the wall, sill and bridge, displacement of the sill relative to facing and also maximum acceleration of the wall and bridge were investigated. Also a three dimensional finite element model of a GRS abutment bridge system was created to study the seismic behavior of the full scale structure subjected to earthquake loading in both longitudinal and transverse directions.

The parametric analysis performed in the present study indicated that GRS abutments can withstand large earthquakes without exerting excessive stresses on the bridge superstructure.

TABLE OF CONTENTS

LIST OF FIGURES

LIST OF TABLES

ACKNOWLEDGMENTS

This work was sponsored by the American Association of State Highway and Transportation Officials (AASHTO), in cooperation with the Federal Highway Administration, and was conducted in the National Cooperative Highway Research Program (NCHRP), which is administered by the Transportation Research Board (TRB) of the National Academies

I express my gratitude to my advisor, Professor Sam Helwany, for his continuous guidance, patience, support, and valuable discussions. His high standards on research and teaching and his commitment towards students made it a privilege to work with him.

I sincerely appreciate my dissertation committee members: Professor Al Ghorbanpoor, Professor Rani El-Hajjar, Professor Anoop Dhingra and Professor Sun Lijing for their support, comments and insights. I express my special thanks to the laboratory staff, Mr. Rahim Reshadi for technical assistance during the experiments.

Finally, special thanks go to my Parents for their unconditional love and support.

Chapter 1- Introduction

1-1 Problem Statement

Over the past two decades, the technology of reinforced soil with geosynthetics as reinforcement has seen applications in the construction of many types of earth structures, including retaining walls, embankments, slopes, and shallow foundations. In actual construction, these reinforced soil structures have demonstrated many distinct advantages over their conventional counterparts. Reinforced soil structures with geosynthetics as reinforcement are typically more ductile, more flexible (hence more tolerant to differential settlement), more adaptable to low quality backfill, easier to construct, require less over-excavation, and more economical (Wu, 1994; Holtz et al., 1997; Bathurst et al., 1997).

Applications of the technology of reinforced soil structures with geosynthetics as reinforcement have been applied to bridge-supporting structures at increasing rate. Depending on the facing rigidity, reinforced soil bridge-supporting structures can be grouped into two types: "rigid" facing structures and "flexible" facing structures. The "rigid" facing is typically a continuous reinforced concrete panel, either precast or cast-in-place. The "flexible" facing, on the other hand, may take the form of wrapped geosynthetic sheets, dry-stacked concrete modular blocks, timbers, natural rocks, or gabions.

The Federal Highway Administration (FHWA) recently developed a reinforced soil wall system for bridge abutment, called Geosynthetic Reinforced Soil – Integrated Bridge System (GRS-IBS), in which the term GRS is strictly used for geosynthetic reinforced soil mass with closely

spaced reinforcement (spacing ≤ 0.3 m). In this study the FHWA's definition is adopted. Note that in the literature the term GRS has sometimes been referred to all geosynthetic reinforced soil structures regardless of reinforcement spacing.

Figure 1 shows a schematic diagram of a typical GRS bridge abutment with segmental concrete block facing. The abutment has four major components: (a) a GRS load-bearing wall (the lower wall), (b) a back wall (the upper wall), which may or may not be a reinforced soil wall, (c) a bridge sill, i.e., a footing to support bridge loads, and (d) segmental concrete block wall facing.

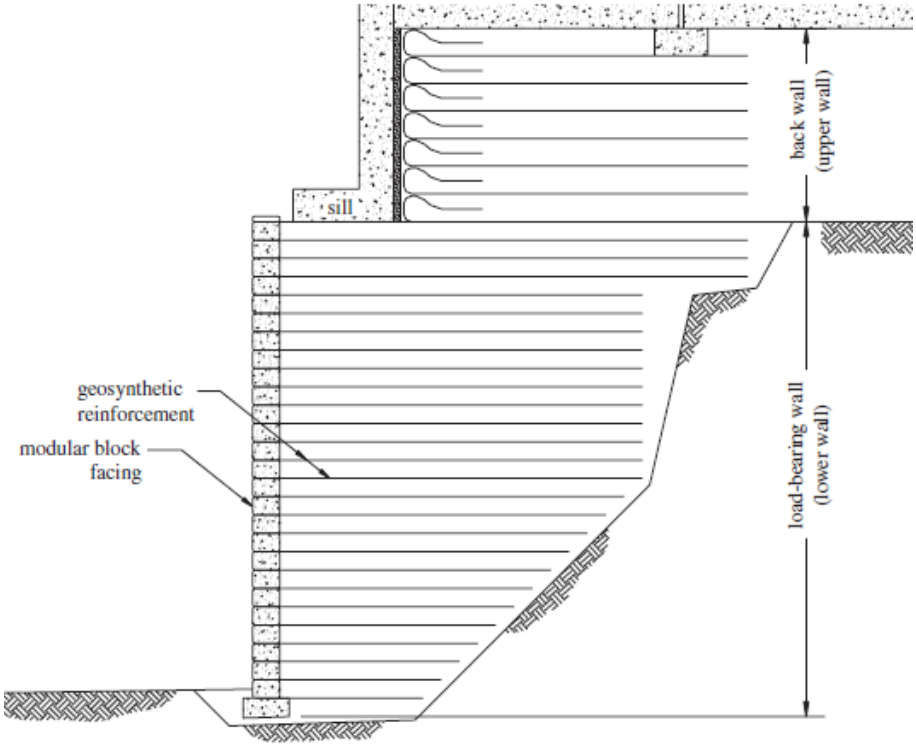

Figure 1-1: Typical GRS bridge abutment with a segmental concrete block facing

When properly designed and constructed, GRS abutments are remarkably stable. They have higher ductility (i.e., less likely to experience a sudden catastrophic collapse) than conventional reinforced concrete abutments. They can also alleviate the bridge "bumps" commonly occurring at the two

ends of a pile-supported bridge with conventional reinforced concrete abutments. In addition, GRS abutments do not require embedment into the foundation soil for stability. This advantage is especially important when an environmental problem, such as excavation into previously contaminated soil, is involved. Construction of GRS abutments is rapid and requires only ordinary construction equipment. They are generally much less expensive to construct than their conventional counterparts

1-2 Need for Seismic Design and Construction Guidelines

Guidelines for design and construction of Geosynthetic reinforced Soil (GRS) bridge abutments with flexible facing that are under predominantly static loading have been developed by Wu et al (2006). Since then, several GRS bridge abutments have been constructed including the GRS abutments in Defiance County, Ohio. Despite great promise of excellent performance characteristics of these GRS abutments under static loads, their response under earthquake loading remained a concern. In order to advance and implement this new technology, especially in seismically active regions, this research was undertaken to examine the performance of GRS abutments under seismic loads in a rational and critical manner.

This research is focused on single span, simply supported bridges. The current seismic design methods, including pseudo-static and displacement methods, are not specifically developed for GRS bridge abutments where the foundation of the bridge superstructure is placed on the top surface of the GRS abutment and generally is subjected to large, sustained and often eccentric

loads. This study is aimed to predict the seismic behavior of GRS bridge abutments with modular block facing.

1-3 Research scope

In order to study the seismic behavior of GRS bridge abutments with modular block facing the following tasks was performed:

- Literature Review.
- Material characterization including selecting proper models for backfill, concrete and geosynthetic
- Laboratory testing in order to determine material parameters used in the finite element model.
- Represent the stress-Strain behavior of the selected material models using the determined material parameters.
- Describing the shake table test of a full scale GRS bridge abutment performed by Helwany et al.
- Finite element simulation of the full scale shake table test using program LS-DYNA and compare the experimental results with the finite element results in order to verify the FEM model of the GRS bridge abutment.
- Parametric study to investigate the model's response to an actual earthquake with variations such as soil strength, reinforcement spacing, reinforcement stiffness and wall height.

- Creating a three dimensional bridge system model to study the effect of earthquake direction on GRS bridge abutment system.

1-4 Outline of The Dissertation

Chapter 1: Introduction

Chapter 2: Literature Review

This research began with the literature review of the experimental and analytical studies on GRS retaining walls and bridge abutments.

Chapter 3: Material Characterization

Chapter 3 describes the material models used to represent the behavior of the components of a GRS bridge abutment system in the finite element model. The lab experiments and the process of determining material parameters are presented in detail. In this study the material model selected for the backfill is Kinematic Hardening Cap Model. Geotextile reinforcement was represented by the Elastic Plastic Model with Kinematic Hardening and the facing concrete blocks was simulated using Linear Elastic model.

Chapter 4: Shake Table Test and Results

Results of a large scale shake table test conducted by Helwany, et.al at Engineering Research and Development center of U.S. Army's Construction Engineering Research Laboratory in Urbana, Illinois' are presented in Chapter 4. The test was performed to measure the model abutment's response to dynamic loading. The GRS abutment was subjected to five consequent input motions

each for duration of 20 seconds with the amplitudes of 0.17g, 0.3g, 0.45g, 0.67g and 1.0g. The GRS abutment exhibited very good performance under the seismic loading with little to no damage to the abutment until the acceleration reached 0.67g at which point some minor damage began to show at the facing blocks of the bottom corners of the model GRS abutment. Even after the load was increased to 1.0g level, the model remained stable and functional experiencing small permanent horizontal and vertical deformation. The results of the shake table test were used to validate a finite element model of the GRS abutment with modular block facing. The results of the shake table test and finite element model are compared in chapter 4. A good agreement was found between experimental and finite element results.

Chapter 5: Parametric Analysis

Chapter 5 describes the results of the parametric study in which the finite element model of the shake table test abutment is subjected to actual acceleration histories of Kobe1995 and Northridge1994 earthquakes. The influence of soil friction angle, geotextile stiffness, geotextile spacing and bridge height as design variables are investigated. The response of the model abutment including the maximum and permanent lateral displacement of the wall, sill and bridge, displacement of the sill relative to facing and also maximum acceleration of the wall and bridge were investigated. Also the seismic behavior of a three dimensional bridge abutment system subjected to earthquake loading in both longitudinal and transverse directions is presented.

Chapter **6: Summary and Conclusions**

Summary of the dissertation and important findings and conclusions are presented in chapter 6.

Chapter 2: Literature Review

The effective performance of GRS retaining walls during earthquakes has been reported in the literature. Several researchers have reported on the dynamic behavior of Geosynthetic Reinforced Soil Retaining Walls. Some of these studies are presented in the following section.

2-1 Experimental Studies

Richardson and Lee (1975) suggested seismic design method for reinforced earth retaining walls based on the results of shaking table tests on reduced scale (300 mm and 380mm high) reinforced soil walls. This study was followed by testing of a m high steel reinforced soil wall subjected to low strain level forced vibration and high strain level explosive tests (Richardson et al. 1977).

Koga et al. (1988) studied the 14 cases of model shaking table tests of reinforced embankments, made in a steel box of 8m long, 2m high and 1m wide. The backfill soil was made of air dried sand (SP) with the moisture content of 6 to 12 percent and relative density of 50 percent. Reinforcement layers used were Nonwoven Fabrics, plastic nets and steel bars of 0.32 to 2.25m long with the vertical spacing of 10 to 20cm and the overlap length of 30cm. Nonwoven fabrics and plastic nets were fixed to the bed slopes using 15cm long nail .Steel bars were penetrated by 30cm to the bed slope. The input excitation was a 10sec sinusoidal wave loading with the frequency of 4Hz and the excitation acceleration of 100 to 800 gal.

It was concluded that a reinforced embankment has a fairly large seismic resistance if a reinforcing element with a large tensile stiffness is effectively fixed to a bed slope and the slope protection to prevent a local slope failure was critical.

Murata et. al. (1994) performed a large scale shaking table test on a 248cm high geosynthetic reinforced soil retaining wall with full height rigid facing. The backfill soil was made of Inagi sand with degree of compaction of 90.4% and fine content of 16%, compacted at 15 cm lifts. The reinforcements were 1.0m long geogrids with tensile rupture strength of 1.0tf/m. The reinforced soil retaining wall was subjected to dynamic loading in three phases. During the first phase, the shake table was subjected to nine stages of horizontal sinusoidal loading at a frequency of 3.4 Hz for a duration of 20 seconds. The acceleration was increased from 100 gals to 500 gals. At the second phase of loading, a horizontal component of a of an earthquake motion was applied for the duration of two minutes. At the third phase of loading, in order to test the soil for liquefaction, the base sand layer was saturated and then subjected to two steps of sinusoidal motion, at a frequency of 2.0 Hz and maximum acceleration of 200 and 400 gals for the duration of three minutes. The test results showed that the GRS retaining walls with a continuous rigid facing was very stable against earthquake loading and the wall exhibited an approximately monolith behavior during large dynamic loading. The wall was stable even when the supporting sand deposit was liquefied.

Sakaguchi, M. et al. (1996) studied a series of large scale shaking table and reduced scale centrifuge tests to investigate the effects of soil density, geosynthetic length and strength on the magnitude of horizontal wall displacements of geosynthetic reinforced retaining walls under earthquake loading. Large scale shaking table tests were performed on one geogrid reinforced

and three unreinforced models of 1.5 m high model walls placed in a container of the dimensions of 4.0m long, 0.9m wide and 2.0m high. The backfill soil was made of standard laboratory silica sand and five layers of 0.3m long geogrid reinforcements. Cement coated foam were used as light weight facing blocks. The applied excitation was a sinusoidal horizontal acceleration at a frequency of 4Hz. The horizontal displacement amplitude was first set to give a peak base input horizontal acceleration of 40 gal and after 25 cycles of shaking the model was returned to a static loading condition. The peak base horizontal acceleration amplitude was then increased from 40 to 80 gal and the same procedure repeated until a peak base input acceleration of 720 gal was reached.It was concluded that geosynthetic reinforced walls were highly earthquake resistant and a peak base input acceleration of 320 gal was the boundary between stable behavior and yielding of the wall models Furthermore horizontal displacement of steep slopes and walls can be effectively reduced by employing a light weight rigid wall facing.

Matsuo et.al. (1998) performed shake table test on six geosynthetic reinforced soil retaining wall models to observe the behavior and reinforcement mechanism that occur in GRS-RWs. The backfill material used in this study was Air dried Toyoura Sand compacted in 10cm thick layers with relative density of 60% and water content of 16%. The model walls were 1m and 1.4m high with discrete and continuous panels as facing. Five and seven layers of geogrid reinforcements with the length of 40cm,55cm and 70cm with vertical spacing of 20cm were used. Five model walls were subjected to 20 cycles of Sinusoidal motion with a frequency of 5 Hz and one model wall was subjected to the earthquake record of the N-S component recorded by the Kobe Maritime observatory during the Hyogoken Nanbu earthquk.(original peak ground acceleration, PGA=818 cm/s^2). The test models were analyzed using a pseudo-static seismic stability analysis method and permanent displacement method and test results were compared with the analyses

results. The analysis showed that the design method provides a margin of safety against the failure of reinforced soil walls and the sliding block method has the potential to estimate the permanent displacement of GRS retaining walls.

Koseki et al. (1998) performed shaking table tests of small scale (500 mm high) GRS retaining walls with a full height rigid facing and conventional type retaining walls and evaluated the seismic performance of different types of walls. They reported that overturning with tilting of the wall face was the major mode of failure and the walls with longer reinforcement at higher wall levels had improved resistance against overturning.

Bathurs et. al. (2002) studied the seismic behavior of reinforced soil walls with different toe boundary conditions using reduced scale shake table tests. The model walls were 1m high with the reinforcement length and spacing equal to 0.6H and 0.2m respectively. Two types of hinged toe (restrained in vertical and horizontal directions) and sliding toe (restrained in vertical direction) were used. The backfill material was artificial uniformly graded sand with unit weight of 15.7 KN/m3 and a knitted geogrid polyester product was used for reinforcements. It was found that using hinged toe, reduced the magnitude of lateral wall displacements and total load in the reinforcements. Also it was found that the vertical loads on the facing toe were greater than the weight of the facing panel

El-Emam and Bathurst (2004) performed reduced-scale shaking table tests on 1 m high reinforced soil retaining walls to investigate the response of reinforced soil retaining walls to base acceleration. The test results were compared with numerical results developed using the program FLAC. The study showed the stability of the wall is affected by the toe boundary

condition and also the size of the soil failure zone was underestimated by the pseudo-static design methods

Perez and Holtz (2004) conducted a series of shaking table tests on 1.2 m high slopes with a wrapped faced at a slope of 63°. Test results indicated that the failure surface was bi-linear in all cases and increasing the length and strength of the reinforcement and decreasing the reinforcement spacing improved the seismic performance of the slopes.

Ling et al. (2005) performed a large scale shake table test on modular block reinforced soil retaining walls to study the their seismic performance and also to create data for validation of numerical modeling GRS retaining walls. they tested three 2.8m high walls. The reinforcement spacing was 40 cm in two walls and 60cm in one wall. The reinforcement length varied between 0.6 H and 0.9 H. Fine sand with medium relative density was used for backfill material and two type of geogrids with ultimate strength of 35 and 20KN/m were used as reinforcement material. And concrete blocks with dimensions of 24cm×30cm×45cm were used as facing. Kobe earthquake was applied as base input motion. Each wall was subjected to a horizontal acceleration of 0.4g followed by 0.8g. The third wall was subjected to both horizontal and vertical accelerations. They concluded that the GRS retaining walls performed well under earthquake loading and their performance was improved by increasing the length of the top reinforcement layer, reducing vertical spacing of the reinforcements and grouting the top blocks. It was also observed that the lateral displacement was largest at the top of the wall. (2)

Murali and Madhavi (2007) studied the seismic response of wrap faced geotextile reinforced retaining walls by conducting shaking table tests on nine model walls. Model Retaining walls

were of the dimention of 750mm x 500mm in plan area and 600mm deep, reinforced with 2, 3 or 4 layers of 420mm long, woven polypropylene multifilament geotextile with the tensile strength of 55.16 KN/m with vertical spacing of 150mm, 200mm or 300mm. Each geotextile layer was wrapped at the facing for a length of 150mm. The Surcharge pressure on retaining walls were 0.5, 1 and 2 kPa. Backfill material were Poorly graded sand (SP) with Max and Min dry density of 18 and 15 kN/m3 respectively, specific gravity of 2.64, average unit weight of 16~16.1 kN/m3 and relative density of 34~37%. The dynamic excitation applied to the models was 20 cycles of sinusoidal shaking (Single degree of freedom: Horizontal shaking).The base acceleration was 0.1g, 0.15g and 0.2g and Frequency was varied from 1 to 3 Hz. The results showed that accelerations were amplified at higher elevations, low surcharge pressures and lower number of reinforcing layers for a given height of wall. The acceleration amplification response with change in base shaking frequency clearly indicated the role of the fundamental frequency on the response of the system. The face deformations were high for low frequency shaking, low surcharge pressures, fewer reinforcing layers and high base accelerations. The incremental pressures were observed to increase with an increase in the base motion frequency, and the peak to peak values of horizontal pressures were also high at higher base accelerations.

Sabermahani et al (2009) conducted a series of 1-g shake table tests to study the seismic deformation modes of reinforced soil walls. The physical models were 1m high, made of sand (SP), 10 layers of geosynthetic reinforcement and wrap-around facing. The input motion was a harmonic sinusoidal like harmonic time history. It was found that the seismic response of the wall depends more on the reinforcement stiffness than tensile strength of the wall. They also studied the overturning and bulging deformation modes of facing as well as base sliding. In the

overturning mode, there was no failure in the reinforced zone and in bulging mode, single failure surface formed in the reinforced zone.

Also other researchers performed reduced-scale shaking table tests GRS retaining walls to investigate the seismic performance of these structures (e.g., Wolfe et al. (1978), Sugimoto et al. (1994), Ramakrishnan et al. (1998) and Krishna and Latha (2007)).

Some researchers have conducted centrifuge model tests to study the behavior of GRS retaining walls (e.g., Sakaguchi (1996), Nova Roessig and Sitar (1998), Howard et al. (1998) and Liu et al. (2010))

2-2 Finite Element Studies

Hatami and Bathurst (2000b) studied the seismic response of GRS segmental (modular block) retaining walls. They found that the displacement of the walls subjected to single frequency, harmonic input acceleration was larger than the wall displacements caused by earthquake records with comparable predominant frequencies. They also found that low frequency ground motions with high intensity and strong motion duration values can result in significant structural response magnitude of short period retaining walls.

Helwany et al (2001) studied the seismic behavior of segmental retaining walls. They performed finite element analysis of a 0.9m high segmental wall subjected to seismic load on a shake table at the University of Arizona. The computer program DYNA3D was to for the analyses. The retaining wall was made of silica sand with relative density of 0.67% and five equally spaced polypropylene geotextiles. Ramberg Osgood model was used to simulate the nonlinear hysteretic behavior of soil, and a linear elastic model was used for facing and geotextiles. The calculated

horizontal displacement and acceleration of the wall was in good agreement with the measured data from shake table test.

Ling et al (2004) simulated the behavior of GRS retaining walls using finite element method. They utilized computer program Diana-Swandyne-II for analyzing 2D wall models under plane strain condition. To validate the static analysis, they used the Public Work Research Institute walls (reported by Tajiri et. Al. 1996) and for validation of dynamic analyses, the centrifuge tests of GRS retaining walls (conducted at Tokyo Institute of Technology, 1999) were used. The walls were subjected to 20 cycles sinusoidal wave with a frequency of 2-Hz and acceleration amplitude of 0.2g. The backfill material was modeled using a generalized plasticity soil model and the reinforcements were modeled using bounding surface model. It was concluded that increasing length and reducing the spacing of reinforcements, reduced the wall deformation and strains in the reinforcements. But the reinforcement layout had a minimum effect on the amplification of the acceleration.

Fakharian and Attar (2007) investigated the seismic response of Founder/Meadows GRS segmental bridge abutment. They used the Founder/Meadows segmental bridge abutment at Denver, CO, and also a reduced scale shake table test on a retaining wall at Royal Military College of Canada for numerical model verification using 2D FLAC program. For input base motion, a variable amplitude harmonic ground motion record was used. A nonlinear elastic Mohr-Coulomb model with a tangent shear modulus was used for soil and an elasto plastic model was used for geogrids. Friction angle between soil and geogrid assumed to be 0.75 φ and zero cohesion. They concluded that the maximum facing horizontal displacement occurs at an elevation equivalent to 0.6H where H is the height of the front face of the abutment. And Current

earth pressure theories overestimate the reinforcement tensile load compared to numerical results. They also concluded that the horizontal displacements are larger that vertical displacements and reinforcements are subjected to more significant forces during seismic excitations.(1)

Helwany et al (2007) studied the behavior of geosynthetic reinforced bridge abutments under static loading. They simulated two full scale loading tests of GRS bridge abutments using finite element program Dyna3D. Both GRS abutments were 4.65m high and the reinforcement spacing were 0.2m. backfill soil was modeled using two invariant geological cap model and geosynthetic reinforcement were simulated using an elasto plastic model with failure. The results showed that the performance of GRS abutments can be accurately modeled using finite element method. Also the results of parametric study suggested that increasing the backfill strength, reinforcement stiffness and reducing reinforcement spacing improves the performance of the GRS abutments.

Lee and Chang (2010) conducted a numerical simulation of the shaking table tests of three full-scale GRS walls using the finite element program LS-DYNA. they studied maximum wall displacement, maximum backfill settlement, maximum lateral earth pressure, maximum bearing pressure, maximum reinforcement tensile load, absolute maximum acceleration in reinforced soil zone and absolute maximum acceleration in retained soil zone. they indicated that decreasing reinforcement spacing decreased the wall displacement.

Liu et al (2011) investigated the seismic behavior of geosynthetic reinforced soil (GRS) walls with backfill material containing fine soil with plastic index PI>6. The finite element program ABAQUS was used for analyses and a dynamic centrifuge test was used to validate the finite

element models. The models used for analyses were 8m high with 5.6m long reinforcements. A Viscoplastic model with Drucker-Prager yield criterion and Singh-Mitchell creep equation was used for soil and an Elastoplastic Viscoplastic bounding surface model and 1D bar elements was used for geosynthetics. And linear elastic model was used for facing. The 1995 Kobe earthquake was introduced as input motion. They performed a parametric study and found that walls showed a two-wedge deformation mode. The effect of creep was small and reinforcement load increased by increasing reinforcement stiffness and spacing. Reinforcement length had small effect beyond the slip surface.

Reinforced soil bridge-supporting structures with flexible facing have been the subject of several studies and recently have seen actual applications in the U.S. and abroad, including the Vienna railroad embankment in Austria (Mannsbart and Kropik, 1996), the New South Wales GRS bridge abutments in Australia (Won et al., 1996), the Black Hawk bridge abutments in Colorado, USA (Wu et al., 2001), the Founders/Meadows bridge abutments in Colorado, USA (Abu-Hejleh et al., 2000), the Feather Falls Trail bridge abutments in California (Keller and Devin, 2003), and the Alaska bridge abutments in Alaska (Keller and Devin, 2003). These structures have shown great promise in terms of ductility, flexibility, constructability, and costs.

Chapter 3: Material Characterization

The components of a GRS bridge abutment system include backfill, geosynthetic reinforcement layers and segmental concrete block facing. In this study the material model selected for the backfill is Kinematic Hardening Cap Model. Geotextile reinforcement was represented by the Elastic Plastic Model with Kinematic Hardening and the facing concrete blocks was simulated using Linear Elastic model. In this chapter, a brief description of the material models for the backfill soil and Geotextile reinforcement layers is presented followed by the lab experiments done on soil and geotextile. Then the material parameters are determined based on the test results and the stress-strain behavior of the materials are simulated using the finite element program, LS-DYNA.

3-1 Kinematic Hardening Cap Model

The backfill is represented by the geological cap model. In this model, the two invariant cap theory proposed by Dimaggio and Sandler (1971) is extended to include nonlinear kinematic hardening as suggested by Isenberg, Vaughan, and Sandler 1978. Cap model is situated in the $\sqrt{J_{2D}}$-I_1 stress space, where I_1 is the first invariant of the stress tenor ($I_1 = \sigma_1 + \sigma_2 + \sigma_3$) and $\sqrt{J_{2D}}$ is the square root of the second invariant of the deviatoric stress tensor ($J_{2D} = 1/6\ [(\sigma_1 - \sigma_2)^2 + (\sigma_2 - \sigma_3)^2 + (\sigma_1 - \sigma_3)^2]$). Cap model is consists of three surfaces in $\sqrt{J_{2D}}$ - I_1 space including a failure

envelope surface, f_1, a cap surface, f_2, and a tension cut off surface, f_3. All three surfaces are shown in Figure 3-1.

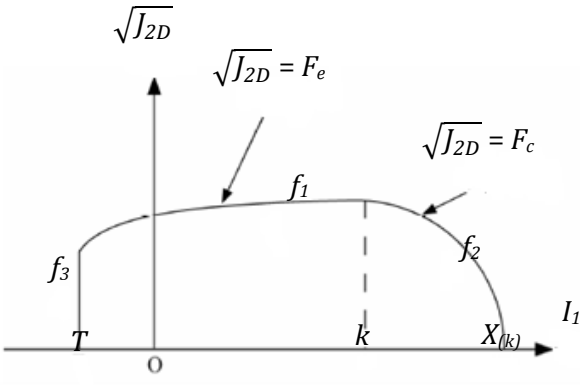

Figure3-1: The Yield Surface of the two invariant cap model in $\sqrt{J_{2D}}$ - I_1 space.

The failure envelope surface, f_1, is given by the expression:

$$f_1 = \sqrt{J_{2D}} - min(F_e(J_1), T_{mises}) \quad (3\text{-}1)$$

Where:

$$f_{e(J_1)} = \alpha - \gamma\, exp(-\beta J_1) + \theta\, J_1 \quad (3\text{-}2)$$

$$T_{mises} = |X(k_n) - L(k_n)| \quad (3\text{-}3)$$

Where α, β, γ and θ are the material parameters. At large values of I_1, the failure surface coincides with the Von-Mises limit which is parallel to the I_1 axes. The yield cap f_2 is a moving yield surface. The moving yield cap follows the shape of an ellipse and is given by:

$$f_2 = \sqrt{J_{2D}} - F_c(J_1, k) \quad (3\text{-}4)$$

Where:

$$F_c(J_1, k) = \frac{1}{R}\sqrt{X(k) - L(k)^2 - [J_1 - L(k)]^2} \quad (3\text{-}5)$$

And $X(k)$ is given by the following function is the intersection of the cap surface with I_1 axis:

$$X(k) = k + R\, F_e(k) \quad (3\text{-}6)$$

$$L(k) = \begin{cases} k & if \;\; k > 0 \\ 0 & if \;\; k \leqslant 0 \end{cases} \quad (3\text{-}7)$$

Where k is the hardening parameter and in Figure 3-1 it's shown as the value of I_1 at the intersection of the cap surface and the failure surface. R is termed the shape factor and is the ratio of the major axis to minor axis of the ellipse: R b = ($X(k)$ - k) and b is the value of $\sqrt{J_{2D}}$ when $I_1 = k$. Note that $X(k)$ is the value of I_1 at the intersection of the yield cap and the I_1-axis $X(k)$ is a hardening parameter that controls the change in size of the moving yield surface and the magnitude of the plastic deformation, and $X(k)$ depends on the plastic volumetric strain ε_v^p through:

$$X(k) = \frac{-1}{D}\ln\left(1 - \frac{\varepsilon_v^P}{W}\right) + X_0 \quad (3\text{-}8)$$

Where D, W, and X_o are the material parameters. Note that W characterizes the ultimate plastic volumetric strain, D denotes the total volumetric plastic strain rate, and X_o determines the initiation of volumetric plastic deformation under hydrostatic loading conditions (Desai and Siriwardane, 1984) and (Zaman et al., 1982). X_0 can also be thought as the preconsolidation hydrostatic pressure.

The tension cut off surface f_3 is given by:

$$f_3 = T - I_1 \quad (3\text{-}9)$$

T: specifies the maximum hydrostatic tension sustainable by the material.

Following the approach of Isenberg et al. (1978), a nonlinear kinematic hardening is included in the model by replacing the stress tensor σ by the translated stress tensor η = σ - α. Where α is a deviatoric history tensor defining the translation of the yield surface in the stress space. Nonlinear hardening low is given by:

$$\alpha = \bar{C}\bar{F}_{(\sigma,\alpha)}\varepsilon^{p} \quad (3\text{-}10)$$

$\bar{C}$ is a constant estimated from the slope of shear stress-plastic shear strain curve at low levels of shear stress. The function $\bar{F}$ is defined as:

$$\bar{F} = max\left(0\ ,1 - \frac{(\sigma-\alpha).\alpha}{2\ N\ F_e(J_1)}\right) \quad (3\text{-}11)$$

Where N is a constant defining the size of the yield surface.

The advantages of the cap model over other pressure dependent plasticity models are the ability to control the amount of dilatancy produced under shear loading and also modeling plastic compaction.

3-2 Experimental work

Laboratory testing of the materials were carried out to obtain results which assisted in determining the model parameters. The experimental program for this study is listed in Table 3-1.

Table 3-1: Experimental tests and expected results

Test	**Result**
Sieve Analysis	Soil classification
Compaction	Maximum Density and Optimum water content
Triaxial Compression Test	Failure Surface Parameters, Young's Modulus
Triaxial Cyclic Test	Kinematic Hardening Parameters
Hydrostatic Compression Test	Hardening cap parameters, Bulk Modulus
Fabric Tensile Strength Test	Plastic- Kinematic model Parameters
Pull Out Test	Concrete block-Geotextile Friction Coefficient

3-2-1 Sieve analysis

Sieve analysis was performed on two soil samples. The grain size distribution curves are shown in Figure 3-2. According to the Unified Soil Classification System (USCS) the soil is classified as poorly graded gravel with sand, GP-GM.

3-2-2 Modified proctor compaction test

From the results of a modified proctor compaction test, the backfill soil had the optimum moisture content of 6.8% and maximum density of 21.52 KN/m^3 .

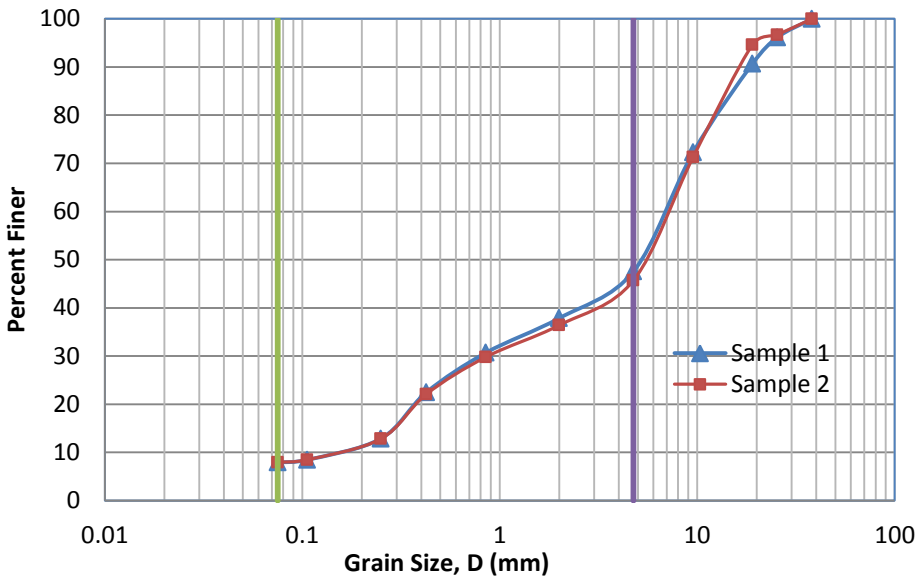

Figure 3-2: Grain size distribution curves

3-2-3 Triaxial Compression Test

Consolidated Drained Triaxial Compression tests were performed at confining pressures of 70 kPa, 140 kPa and 210 kPa. The Soil Samples were cylinders with the diameter of 10 cm and height of 20 cm. The test method was displacement control. The plot of the Shear stress ($\Delta\sigma$) vs. axial strain, ε_1, is shown in Figure 3-3. The slope of the initial portion of the stress-strain curve gives the value of the young's modulus, E.

3-2-4 Triaxial Cyclic Test

Triaxial Cyclic Tests was performed at confining pressures of 70 kPa, 140 kPa and 210 kPai. The deviator stress (σ_1 - σ_3) was increased up to 70% of the shear strength of the soil at the same confining pressure followed by five cycles of unloading-reloading. Figure 3-4 shows the result of a Triaxial Cyclic Test with the confining pressure of 70 kpa.

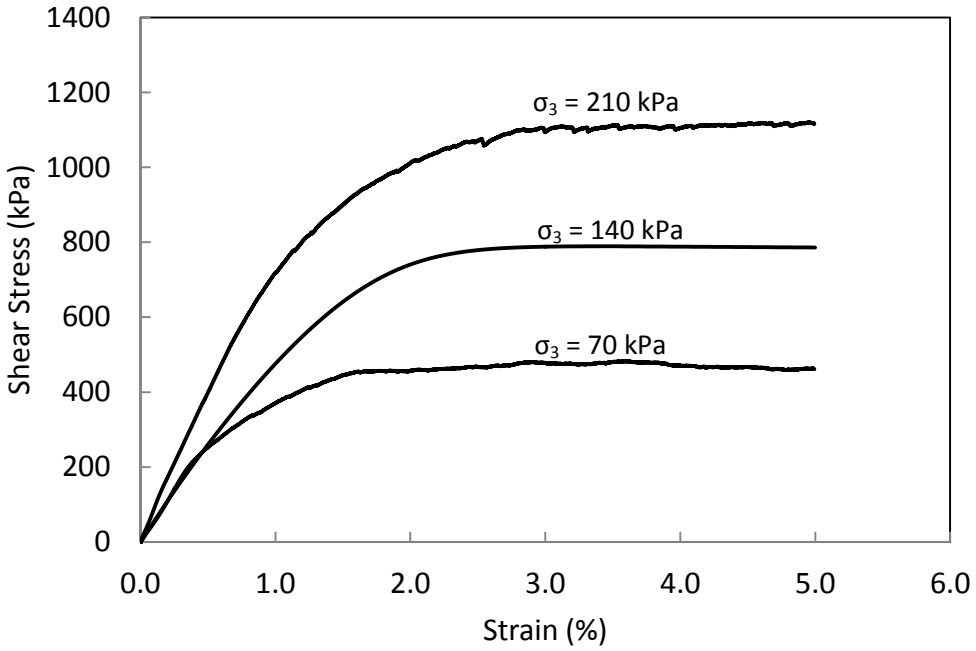

Figure 3-3: Consolidated Drained Triaxial Compression Test results at confining pressures of 10, 20 and 30 psi

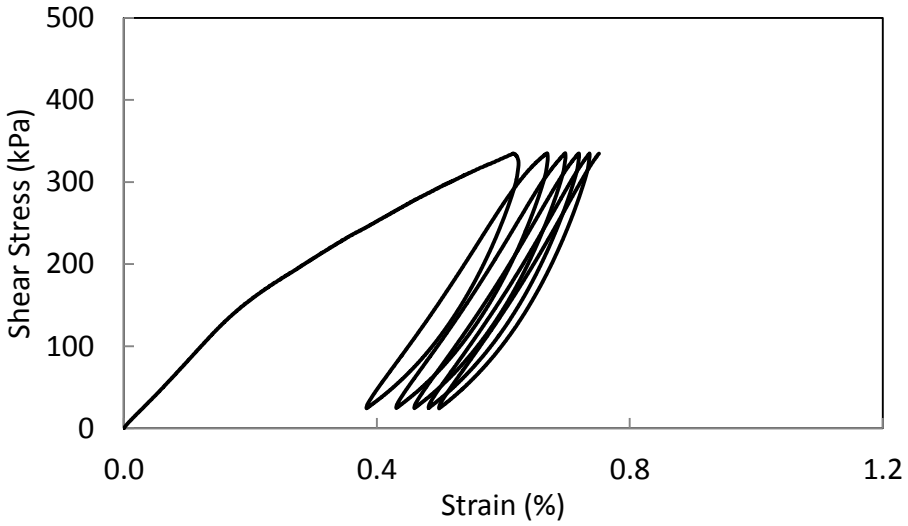

Figure 3-4: Deviatoric Stress vs. Axial Strain plot obtained from the Triaxial Cyclic Test with the confining pressure of 10 psi

3-2-5 Hydrostatic Compression Test

The Hydrostatic Compression (HC) test was performed on soil samples with the diameter of 10 cm and height of 20 cm as shown in Figure 3-5. The slope of the unloading curve gives the bulk modulus K. Also cap model parameters were determined using the results of the HC test.

3-3 Determination of the Kinematic Hardening Cap Model Parameters of Soil:

The Kinematic Hardening Cap Model Parameters and the required tests to experimentally determine each parameter are shown in Table 3-2:

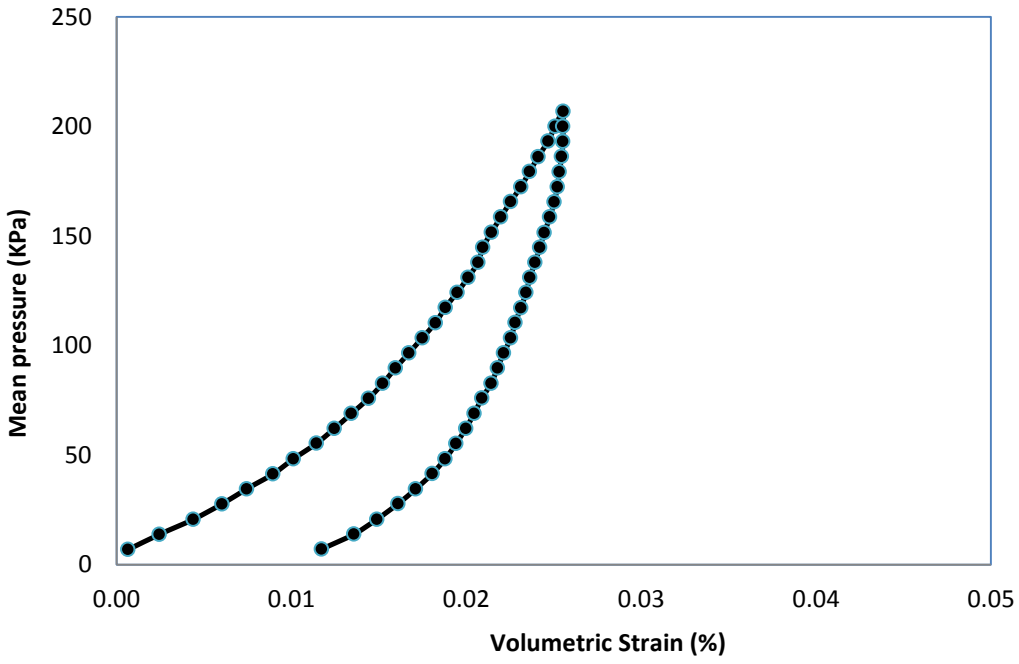

Figure 3-5: Hydrostatic Compression test result

Table 3-2: Kinematic Hardening Cap Model Parameters and the required tests

	Parameter	**Description**	**Required test**
Elastic parameters	K	Bulk Modulus	Hydrostatic compression
	G	Shear Modulus	Triaxial Compression
	v	Poisson's ratio	Correlation
Yield Surface Parameters	α	Failure envelope parameter	Triaxial Compression
	θ	Failure envelope linear coefficient	Triaxial Compression
	γ	Failure envelope exponential coefficient	Triaxial Compression
	β	Failure envelope exponent	Triaxial Compression
Cap model hardening	D	Hardening law exponent	Hydrostatic compression
	W	Hardening law coefficient	Hydrostatic compression
	R	Shape factor	Hydrostatic compression
	X_o	Initial cap	Hydrostatic compression
Kinematic Hardening Parameters	C	Kinematic Hardening coefficient	Cyclic Triaxial Test
	N	Kinematic Hardening Parameter	Cyclic Triaxial Test

3-3-1 Determination of Elastic parameters

The Bulk Modulus, K, is calculated from the Hydrostatic compression test result. The Slope of the unloading curve of the of the mean pressure, P, vs. volumetric strain, ε_v, gives the Bulk Modulus, K. The Young's Modulus, E, can be determined from the results of triaxial compression tests. Young's Modulus can be calculated from the initial slope of the Shear stress,

(σ_1-σ_3), vs. axial strain, ε_1, The Bulk Modulus and the shear modulus are related to the Young's Modulus and Poisson's ratio through the following equations:

$$K = \frac{E}{3(1-2\nu)} \quad (3\text{-}12)$$

$$G = \frac{E}{2(1+\nu)} \quad (3\text{-}13)$$

$$G = \frac{3(1-2\nu)\,K}{2(1+\nu)} \quad (3\text{-}14)$$

3-3-2 Determination of yield surface parameters

The expression for the yield surface, f_1, is given as

$$f_1 = \sqrt{J_{2D}} + \gamma e^{-\beta J_1} - \theta J_1 - \alpha = 0 \quad (3\text{-}15)$$

Assuming a linear yield surface equation reduces to:

$$f_1 = \sqrt{J_{2D}} - \theta I_1 - \alpha = 0 \quad (3\text{-}16)$$

This equation represents Drucker-Prager yield surface and its slope and its intercept with the $\sqrt{J_{2D}}$ axis gives parameter $\theta = 0.35$ and $\alpha = 32$ kPa respectively which can be calculated using the Triaxial Compression Test results:

$$\begin{cases} (\sigma_3 , \sigma_1) = (70\text{ kPa}, 470\text{ kPa}) \rightarrow (I_1 , \sqrt{J_{2D}}) = (610 , 231) \\ (\sigma_3 , \sigma_1) = (140\text{ kPa}, 755\text{ kPa}) \rightarrow (I_1 , \sqrt{J_{2D}}) = (1035 , 355) \\ (\sigma_3 , \sigma_1) = (210\text{ kPa}, 1105\text{ kPa}) \rightarrow (I_1 , \sqrt{J_{2D}}) = (1525 , 517) \end{cases}$$

Figure 3-6 shows the liner yield surface fitted to the points obtained from the test results.

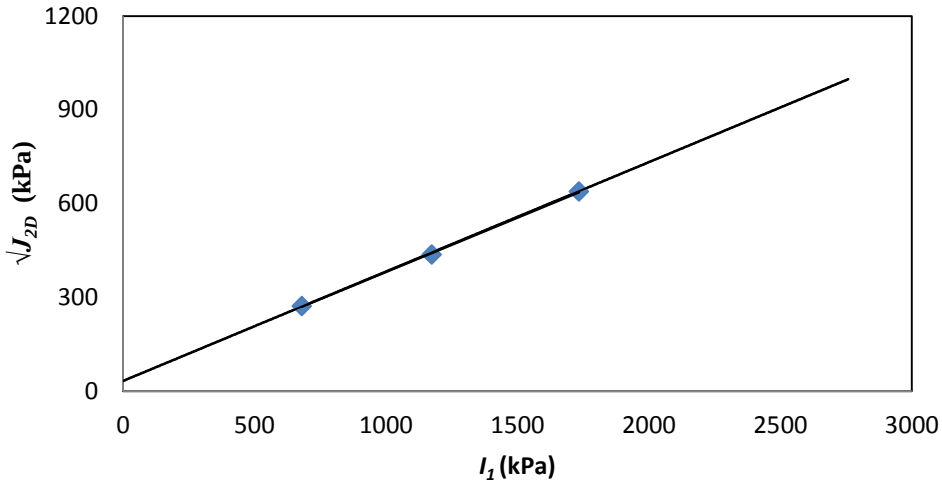

Figure 3-6: The linear yield surface in the stress space of I_1 vs. $\sqrt{J_{2D}}$

3-3-3 Determination of the Cap Model Hardening parameters

The values of D, W and X_0 should be calculated using hardening rule:

$$X(k) = -\frac{1}{D}\ln\left(1-\frac{\varepsilon_v^P}{W}\right)+X_0 \qquad (3\text{-}17)$$

It's assumed that the value of X_0 is zero, which means that hardening starts the moment the material is loaded and there is no initial yield cap. Most soils show plastic deformation at very low stress levels, hence it is reasonable to assume that X_0 is equal to zero in most soils.

Parameters D and W can be found from the mean pressure, P, vs. volumetric strain, ε_v, plot obtained from the hydrostatic $_{compression}$ test result. Substituting X_0 = 0, $X(k)$=3P, where P is the mean pressure and rearranging we have:

$$\varepsilon_v^p = W(1 - e^{-3PD}) \quad (3\text{-}18)$$

Note that at the confining pressure stage, Shear stress is zero and I_1 is simply reduced to 3P. Also the total volumetric strain is the sum of plastic volumetric strain and elastic volumetric strain, so plastic volumetric strain can be expressed as:

$$\varepsilon_v^p = \varepsilon_v - \varepsilon_v^e \quad (3\text{-}19)$$

Calculating elastic volumetric strain using bulk modulus we have:

$$\varepsilon_v = W(1 - e^{-3PD}) + \frac{P}{K_t} \quad (3\text{-}20)$$

Parameters D and W can be found by trial and error so that equation (3-20) can closely predict the mean pressure vs. volumetric strain plot resulted from the hydrostatic compression test. Figure 3-7 shows the mean pressure vs. volumetric strain plot and the curve predicted using equation (3-20).

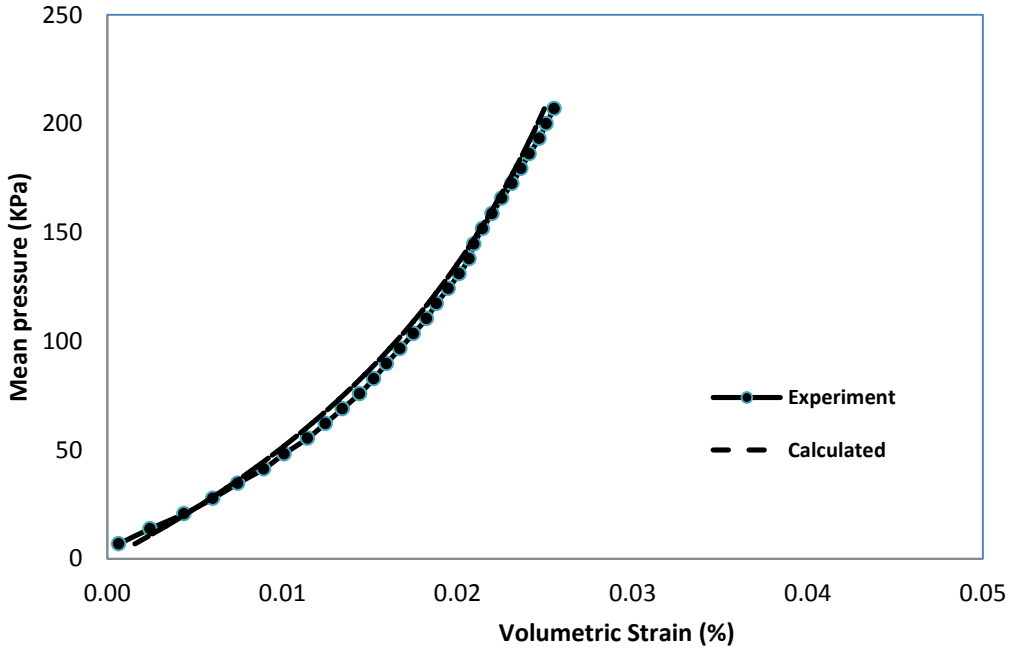

Figure 3-7: Mean pressure vs. volumetric strain plot obtained from the HC test and the equation (3-20).

The parameter R is the average ratio of the major to minor axis of the elliptical hardening or yield caps. The yield caps are contours of equal volumetric plastic strains. So, in order to plot the caps the values of volumetric plastic strain increments $d\varepsilon_v^P$ have to be determined. Parameters for representing geological cap model are summarized in Table 3-3.

3-4- Finite Element Simulation of Soil

The stress-strain behavior of the model components including backfill soil and geosynthetic reinforcement are simulated using finite element program LS-DYNA.

Figure 3-8 shows the simulation of Triaxial Compression Test performed on three cylindrical soil samples with the height of 20 cm and diameter of 10 cm. For this simulation a one element model can also be used which gives very close results as the full scale soil sample. In one element model, $1/8^{th}$ of the soil sample is considered and three faces of the element are planes of symmetry. In both models 8 node solid elements are used. In this simulation the confining pressure is applied as a constant load and then the top surface of the soil sample is subjected to a linearly increasing displacement. In Cyclic Triaxial Tests, the samples are loaded to 70% of the shear strength of the soil which is obtained from the triaxial compression test at the same confining pressure, followed by five cycles of unloading-reloading. Table 3-4 shows the values of the soil parameters used in this simulation.

The stress-strain behavior of the soil, obtained from the finite element model are compared to the experimental results in figure 3-9. The result of the triaxial cyclic test is also compared to the experimental result in figure 3-10.

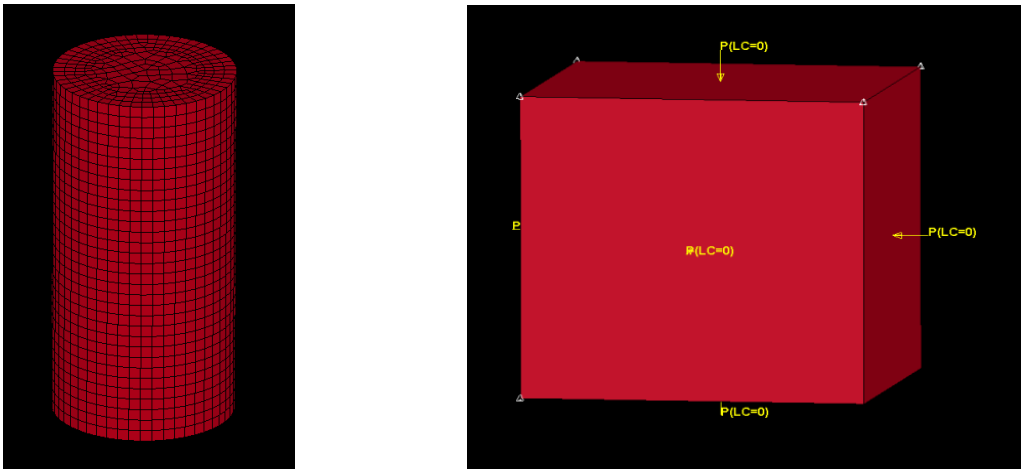

(a) (b)

Figure 3-8: Simulation of Triaxial Compression Test on soil samples using LS-DYNA, (a) Full scale soil sample, (b) 1 element simulation.

Table 3-3: Values of the soil parameters used in FEM simulation

	Parameter	**Value**	**Unit**	**Description**
Elastic parameters	K	10000	psi	Bulk Modulus
	G	4615	psi	Shear Modulus
	ν	0.3	-	Poisson's ratio
Yield Surface Parameters	α	4.7	psi	Failure envelope parameter
	θ	0.35	-	Failure envelope linear coefficient
	γ	0	psi	Failure envelope exponential coefficient
	β	0	1/psi	Failure envelope exponent
Cap Model Hardening Parameters	D	0.002	1/psi	Hardening law exponent
	W	0.01	-	Hardening law coefficient
	R	2.0	-	Shape factor
	X_o	0	psi	Initial cap
Kinematic Hardening Parameters	C	2000	-	Kinematic Hardening coefficient
	N	4.9	-	Kinematic Hardening Parameter

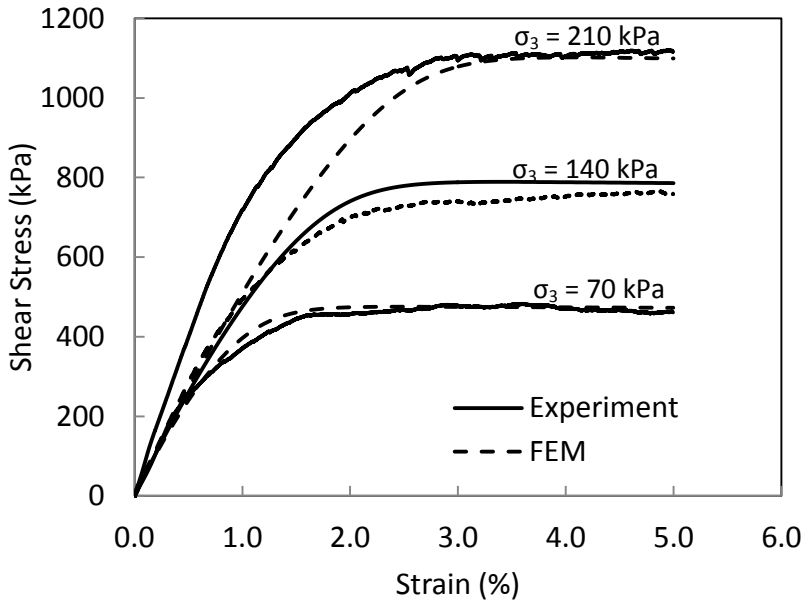

Figure 3-9: Comparison of experimental results and FEM simulation of Triaxial Compression Tests

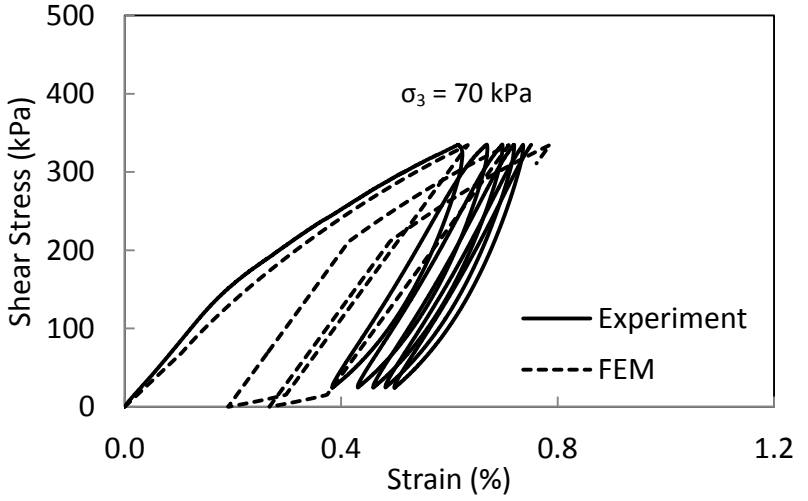

Figure 3-10: Comparison of experimental results and FEM simulation of Cyclic Triaxial Test

3-5- Elastic-Plastic Model with Kinematic Hardening

Plastic- Kinematic model formulated by Krieg and Key (1976) models Isotropic, kinematic or a combination of Isotropic and kinematic with strain rate dependency and failure.

Material failure is realized when the effective plastic strain is equal to the effective plastic strain at failure. When failure occurs, the deviatoric stress components are set to zero.

In the model, the yield condition is given by:

$$\Phi = \bar{\sigma} - \sigma_y\left(\varepsilon_p^{eff}\right) \tag{3-21}$$

Where $\bar{\sigma}$ is the effective stress and σ_y is the current yield stress as a function of plastic effective strain. The effective stress is given by:

$$\bar{\sigma} = \sqrt{\frac{3}{2} S_{ij} S_{ij}} \tag{3-22}$$

Where S_{ij} is the deviatoric stress tensor.

The isotropic hardening low is given by :

$$\sigma_y = \left(1 + \left(\frac{\varepsilon}{C}\right)^{1/P}\right)\left(\sigma_0 + \beta E_P \varepsilon_P^{eff}\right) \tag{3-23}$$

Where σ_0 is the initial yield stress, $\dot{\varepsilon}$ is the strain rate, C and P are the Cowper-Symonds strain rate parameters, ε_P^{eff} is the effective plastic strain, and E_P is the plastic hardening modulus which is given by:

$$E_p = \frac{E_{tan} E}{E - E_{tan}} \tag{3-24}$$

Isotropic and kinematic contributions may be varied by adjusting the hardening parameter β between 0 (kinematic hardening only) and 1 (Isotropic hardening only) as shown in figure 3-11. Strain rate is accounted for using the Cowper- Symonds model which scales the yield stress by the strain rate dependent factor as shown in equation 3-14.

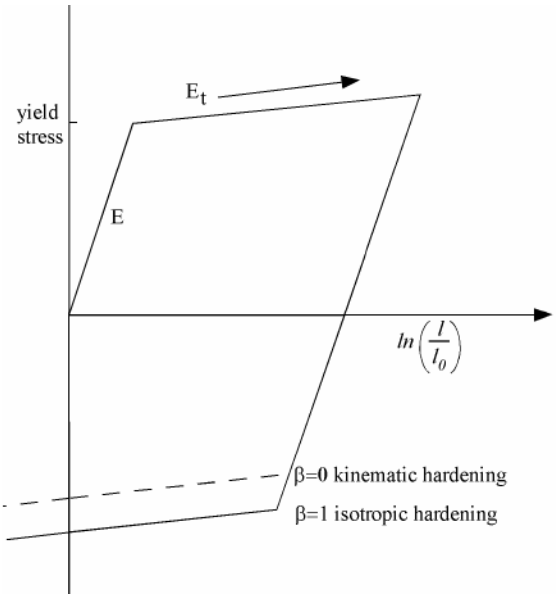

Figure 3-11: Elastic- Plastic behavior with kinematic and isotropic hardening where I_0 and I are undeformed and deformed lengths of uniaxial tension specimen. Et is the slope of the bilinear stress strain curve.

3-6 Determination of Plastic- Kinematic Model parameters for geosynthetic reinforcements

Table 3-4 shows the Plastic- Kinematic Model parameters for geosynthetic reinforcements and the required tests to obtain those parameters:

Table 3-4.: Plastic- Kinematic Model parameters for geosynthetic reinforcements and the required tests to obtain those parameters

Parameter	**Unit**	**Description**	**Required test**
E	psi	Young's Modulus	Tensile Strength
v	-	Poisson's ratio	Tensile Strength
σ_y	psi	Yield Stress	Tensile Strength
E_t	psi	Tangent Modulus	Tensile Strength
$\varepsilon_p^{eff}{}_{(F)}$	-	Effective Plastic Strain at Failure	Calculation
β	-	Hardening Parameter	0-1
C	-	Strain Rate Parameter	0
P	-	Strain Rate Parameter	0

3-6-1 Tensile Strength Test

A tensile stress - strain plot for a geosynthetic reinforcement is shown in Figure 3-12. The curve obtained from the test was estimated by a bilinear stress- strain curve produced by Plastic-Kinematic Model formulation. Then as shown in Figure 3-12, the model parameters including yield stress, Young's modulus and tangent modulus will be determined from the curve. Parameters C and P will be zero, as the rate dependency will not be considered in this study.

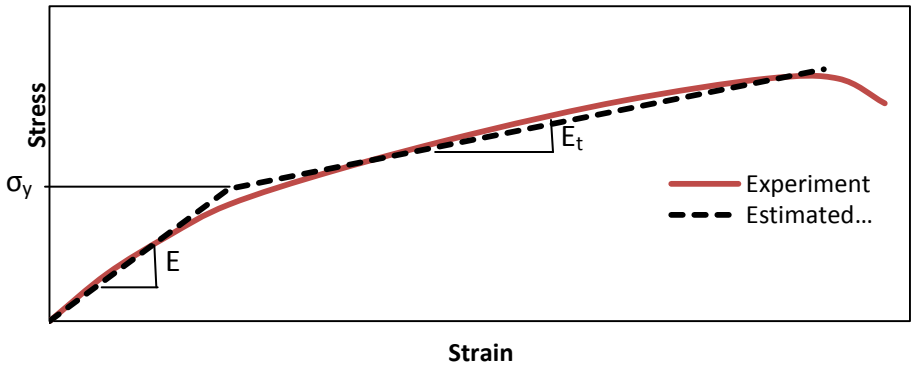

Figure 3-12: The plot of tensile stress- strain for geosynthetic reinforcement obtained from the test and Plastic- Kinematic Model formulation

3-6-2 Friction Coefficient of Soil- Gesynthetic Interface:

A pull-out test was performed to obtain the concrete block- geosynthetic interface shear resistance. This test is schematically shown in Figure 3-13:

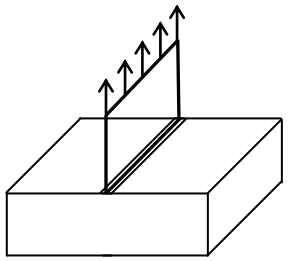

Figure 3-13: Pull out test

The test equipment include an aluminum box with the dimensions of 14 in x 7.5in x 20in in which a geotextile sheet was placed between two concrete facing blocks and the confining pressure was applied through air bags. One end of the geotextile is embedded between the concrete blocks and another end is screwed between two steel bars and is subjected to the tensile

force in the Instron machine. Each concrete block was 36 cm x 19 cm x 10 cm with two square cavities of 16 cm x 16 cm x 10 cm.

The test was performed in three confining pressures of 32.4 kPa, 71 kPa and 99.3 kPa. The plot of tensile force –elongation is presented in Fig.3-14.

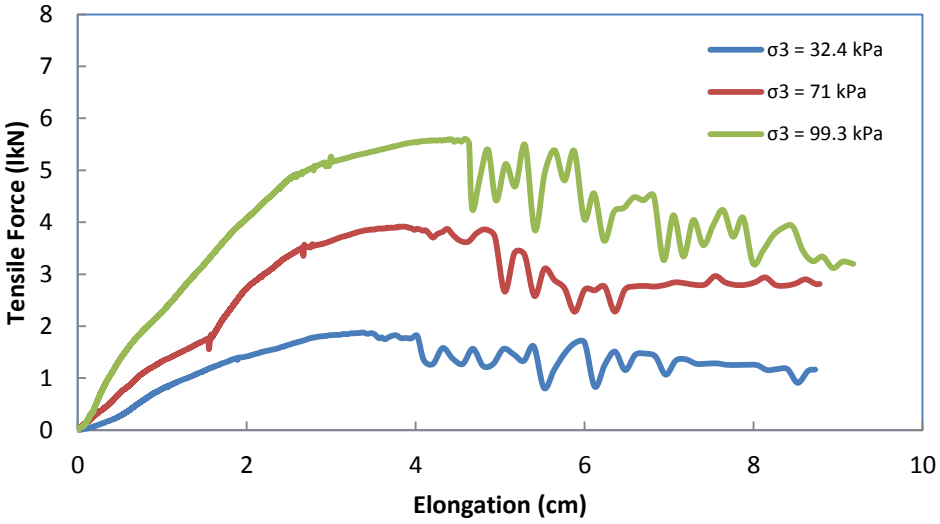

Figure3-14 Plot of Tensile Force-Elongation for pull out tests

Interface shear resistance in the pull out test is given by:

$$\tau = F / (2A) = \sigma_3 \times \mu \rightarrow \quad \mu = F / (2 \times A \times \sigma_3) \qquad (3\text{-}25)$$

Where F is a pull out force, A is the area of the embedded geotextile, σ_3.is the normal stress on the blocks in the form of confining pressure and μ is the friction coefficient of the concrete-geotextile interface. The plot of normal stress-shear stress is presented in figure 3-15. The slope of the line which is 0.77 is the friction coefficient of concrete-geotextile interface.

In the finite element study, the blocks are modeled as solid cubes and the cavities are not considered. In order to keep the shear stress on contact surfaces constant, the friction coefficient of concrete-geotextile interface should reduced to $\mu = 0.35$.

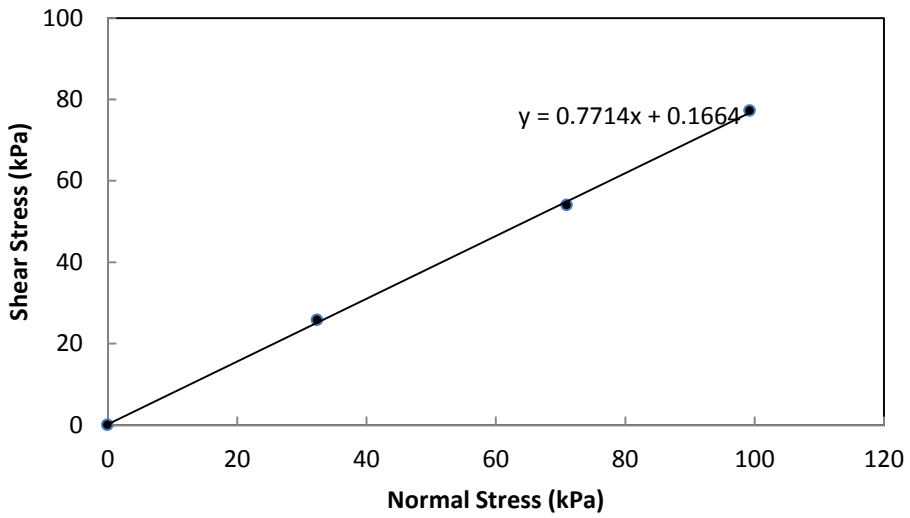

Figure 3-15. The plot of normal stress-shear stress

3-7 Finite Element Simulation of the Geotextile

Figure 3-16 shows the simulation of Tensile Strength Test performed on a Geotextile sample. For this simulation a one element (4 node shell element) model is used. In this simulation one side of the shell element is fixed and other side is subjected to a linearly increasing tensile force. Table 3-5 shows the parameters used in the FEM modeling of Tensile Strength Test.

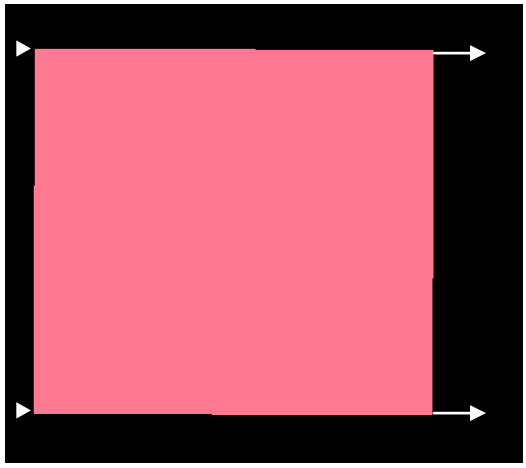

Figure 3-16: Simulation of Tensile Strength Test performed on a Geotextile sample

Table 3-5: Parameters used in the FEM modeling of Tensile Strength Test.

Parameter	**Value**	**Unit**	**Description**
E	95000	psi	Young's Modulus
v	0.3	-	Poisson's ratio
σ_y	1713	psi	Yield Stress
E_t	80000	psi	Tangent Modulus
$\varepsilon_p^{eff}{}_{(F)}$	1.3	-	Effective Plastic Strain at Failure
β	1	-	Hardening Parameter
C	0	-	Strain Rate Parameter
P	0	-	Strain Rate Parameter

The results obtained from the experiment and FEM are compares in Figure 3-17. As the following figure shows, when the geotestile fails, it will not carry any more load and the stress level in the element becomes zero.

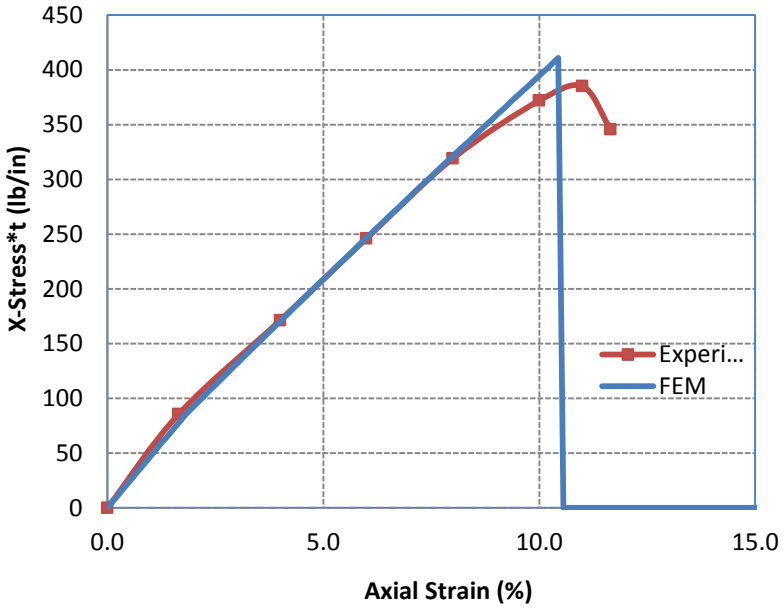

Figure 3-17: Comparison of experimental results and FEM simulation of Tensile Strength Test

Chapter4- Shake Table Test and Results

4-1- Shake Table Test

A full scale GRS bridge abutment shake table test was performed by Helwany et al. (2009) at the U.S. army Engineering Research and Development Center- Construction Engineering Research Laboratory (ERDC-CERL). Testing device was a Triaxial Earthquake and Shock simulator (TESS). Figure 4-1 shows the bare TESS platform before the construction of the model and schematic design of the bridge abutment model is shown in Figure 4-2. The GRS bridge abutment was tested using a staged sinusoidal horizontal motion with increasing amplitude up to 1g. Figure 4-3 shows different stages of the construction of the GRS abutment.

The GRS abutment is 3 m long, 3 m wide and 3 m high. A 20 cm thick foundation soil was placed and compacted in 10 cm lifts. A layer of geotextile fabric (GEOTEX 4x4) was laid below the first course of blocks; the fabric was placed only beneath the block and did not cover the interior soil area. After each layer of block was placed, soil was placed and compacted in two 10 cm lifts using a plate compactor. Engineering and Research International, Inc. measured the moisture content and relative density every 10 cm lift using a nuclear density gauge. The ILDOT CA-6 material used in the GRS abutment had an optimum moisture content of 6.8% and a maximum density of 21.52 kN/m^3 as determined from a modified Proctor compaction test. Lifts were kept above 97% relative compaction throughout the model while the moisture content ranged from 6.4% to 6.9%. After every two lifts of soil placed and compacted, a geotextile layer was placed over the entire soil area and full width of the CMU blocks. The top three courses of

CMU blocks were grouted together for added stability during seismic loading. two elastomeric pads are used to support the bridge at the GRS-abutment end. The other bridge end is supported using two rollers.

Figure 4-4 shows the completed GRS bridge abutment and concrete slabs and steel plates providing the dead load of 445 kN and also simply supported bridge girders.

The sensor types used to measure the response of the bridge abutment included extensometers, 25 accelerometers, 15 linear variable differential transducers, 10 pressure transducers and 20 strain gages. Testing frequencies were 1.5 Hz which was below the natural frequency of the model components and 3 Hz which was higher than the natural frequency of the bearing pad. Test motions are summarized in Table 4-1.

Table 4-1: Test motions of GRS bridge abutment shake table test

Test	**Frequency (Hz)**	**Amplitude (g)**	**Duration (sec.)**
Test 1	1.5	0.17	20
Test 2	3	0.30	20
Test 3	3	0.45	20
Test 4	3	0.67	20
Test 5	3	1	20

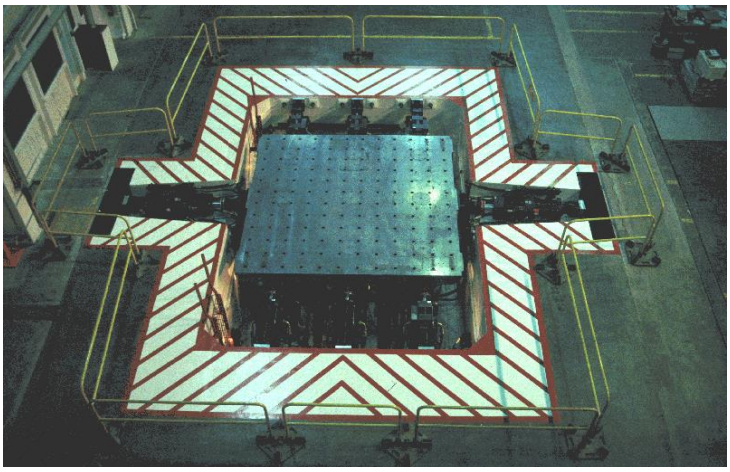

Figure 4-1: The bare TESS platform before the construction of the model

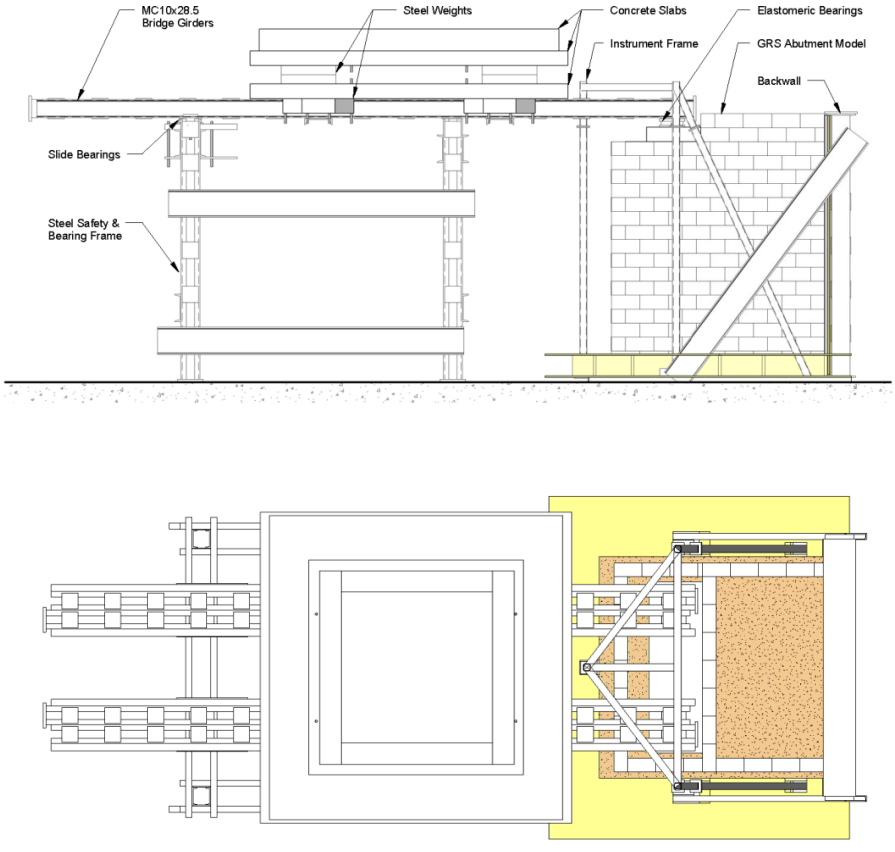

Figure 4-2 Schematic Design of the Bridge Abutment Model

(a)

(b)

(C)

(d)

Figure 4-3: Different stages of the construction of the GRS abutment, (a) Placement and Compaction of the First 10 cm Layer of Soil, (b) First Course of Block Placement, (c) Instrumented Geosynthetic Fabric Placed Above 2nd CMU Course, (d) Completed GRS abutment

Figure 4-4: Completed GRS abutment

System Identification (SI) tests were conducted in order to identify the natural frequency of the GRS bridge abutment system. Figure 4-5 shows the measured horizontal natural frequency of the abutment is approximately 8.5 Hz and the measured horizontal natural frequency of the bearing pad-bridge system was approximately 2.3 Hz which is in close agreement with the 2.24 Hz predicted based on Method B from AASHTO LRFD Bridge Design Specifications (2007). However, any motions at this frequency would create an amplified response. As the sine-sweep motions pass through this frequency the response of the girder and slab system above the model would be amplified, significantly loading the model.

Test results showed that seismic loads having frequencies below the elastomeric pad- bridge natural frequency caused greater vibrations in the bridge and bridge abutment. If the ground motion's frequency is higher than the natural frequency of the bearing pads, the horizontal motion of the superstructure can be isolated from the substructure significantly reducing the horizontal forces placed on the abutment.

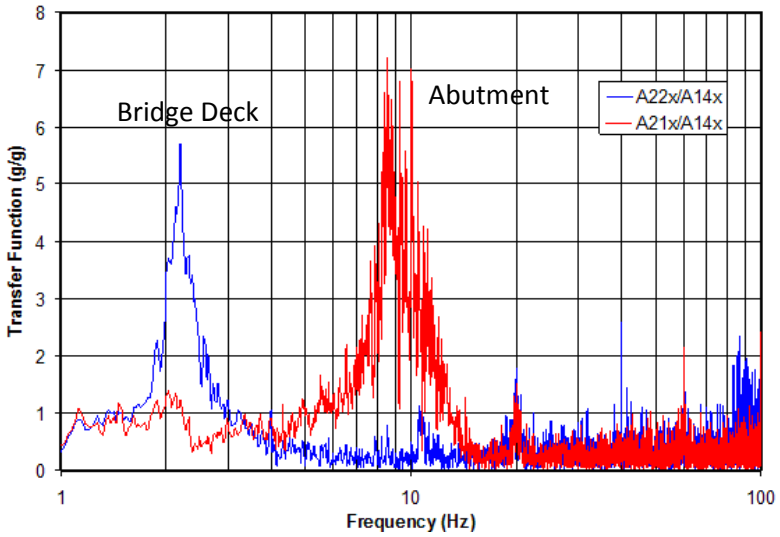

Figure 4-5 Example Plots of Transfer Functions Showing 2.3 Hz and 8.5 Hz Modes (

4-2- Finite Element Simulation of Seismic GRS Test Abutment Experiment

The full scale seismic GRS bridge abutment experiment was simulated using finite element program LS-DYNA. The capability of the computer program for analyzing the seismic performance of segmental facing GRS bridge abutment was evaluated by comparing the analytical results with measured data of the experiment. Three dimensional simulation is presented in detail in the following sections.

4-2-1 Model Configuration

Three dimensional finite element model of the NCHRP seismic GRS abutment experiment is shown in Figure 4-6. The configuration of the GRS abutment constructed on the shake table platform and the detailed geometry is described in section 4-1. In the finite element model, each soil layer, concrete facing block, geotextile reinforcement and other components of the bridge, back wall and shake table are modeled as individual parts which include total 437 parts. Each part is assigned appropriate element type and material model. Element types, Loading and boundary conditions and contact types are described in the following sections.

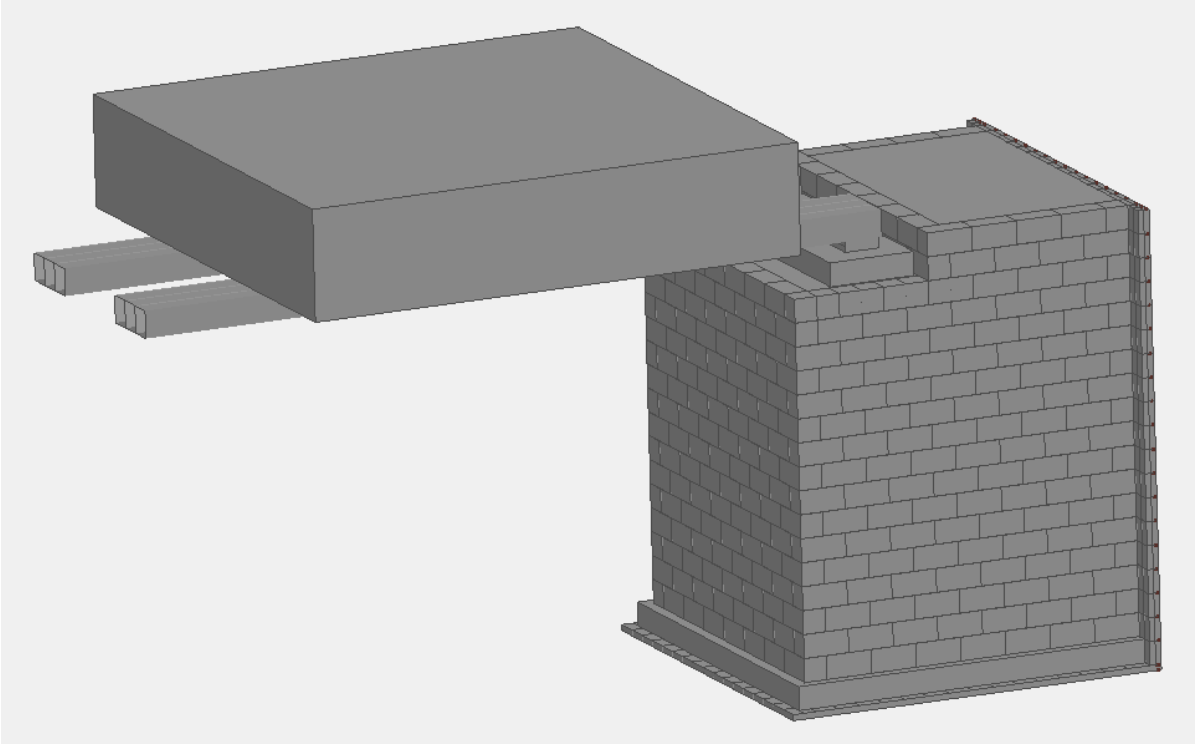

Figure 4-6: FEM simulation of the GRS bridge abutment

4-2-2 Element Types

The soil and facing modular blocks are modeled using 8-node solid break elements with fully integrated selectively-reduced formulation (type 2). The default constant stress solid element was found to have excessive hourglassing. Thus, fully integrated element type was used to totally eliminate the hourglassing effect. The geotextile reinforcements are modeled using the 4-node shell elements with default Belytschko-Tsay element formulation. To eliminate bending resistance, the number of through shell thickness integration points is set to one. Also the girders supporting the dead load of the bridge is created using the same type of shell elements with 2 through thickness integration points. The model includes 437 parts, 9021 solid elements, 7231 shell elements and 2 springs.

The sliding function of elastomeric pads are simulated using springs. The springs are created with discrete elements which allow sliding in the horizontal direction.

4-2-3 Loading and boundary conditions

The GRS abutment model is subjected to gravity loading and sinusoidal input motions. The gravity load is applied as a body load in the vertical (z) direction via a smooth function. The gravitational acceleration increases to 1 g during one second and remains constant for the entire simulation time. The GRS abutment seismic loading according to the NCHRP experiment, consisted of five shaking tests (stages) each lasting 20 seconds. In test 1, the model was subjected to a sinusoidal motion in the longitudinal direction with acceleration amplitude of 0.17 g at 1.5-Hz frequency. In test 2, the amplitude was 0.35 g and the frequency was increased to 3 Hz. Test 3, 4 and 5 were performed at a 3-Hz frequency with amplitudes of 0.45 g, 0.67 g and 1 g respectively. The input acceleration versus time is presented in Figure 4-7.

In the numerical simulation, the translational constraint in the vertical (z) direction is applied to the base of the model and also to the end of the girders. The sinusoidal input motions are simulated by prescribed horizontal motion, applied to the boundary nodes at the base of the model.

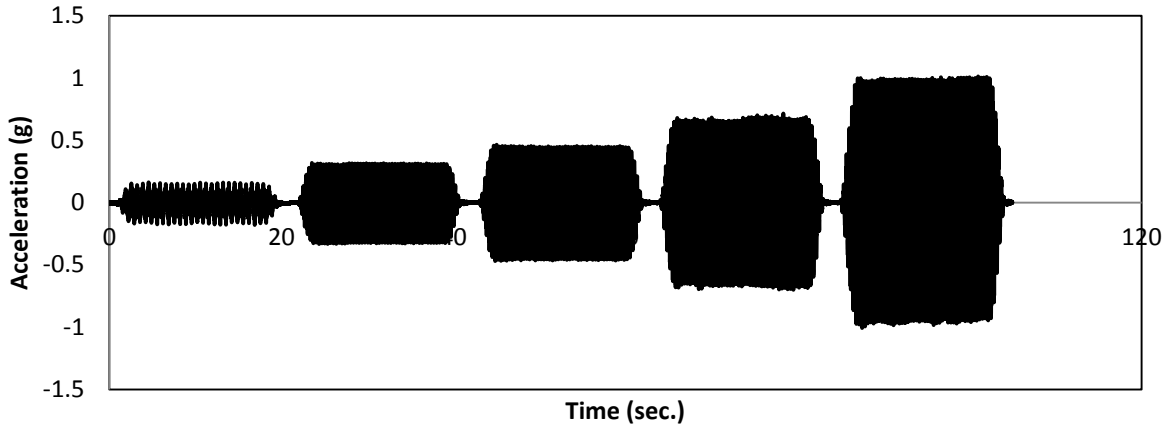

Figure 4-7: Input acceleration for FEM simulation of the GRS bridge abutment

4-2-4 Contact Types

In numerical modeling of the GRS abutment, two contact types are utilized to simulate the interaction between different parts of the model. The first contact type is Automatic-Single Surface-Smooth and the second contact type is Tied Surface to Surface.

The Automatic single surface contact is used for global contact in which the slave surface will include all parts of the model and no master surface is defined. Contact is considered between all parts of the model including self contact of each part. In this simulation, a segment based contact algorithm is used where contact between segments is treated rather than using node to segment treatment. In contact treatment, the penetration of two surfaces is resisted by a force which is represented by linear springs between the slave and master segments. In this simulation, the contact spring stiffness, is calculated based on the nodal masses and the global time step size. This method is suited for contact between materials with very different stiff nesses.

The second contact type used in this analysis is Tied surface to surface. In tied contact types, the slave and master segments are constrained to move together. The rotational degrees of freedom of slave segments are not constrained in this type of contact. In offset tied contact, a penalty base formulation is used and an offset distance between the master and slave segments is permitted. In this FEM model, the top three rows of blocks are tied together and also the dead load and beams, sills and elastomeric pads and table and wall are tied together.

Static and dynamic coefficient of frictions are set equal to avoid numerical noise. Three different values of coefficient of friction (μ) correspond to 1/3 tan φ′, 1/2 tan φ′ and 2/3 tan φ′ were tested for calibration study where φ′ is the friction angle of the backfill equals to 44° and coefficient of friction corresponding to 1/2 tan φ′ is in best agreement with the experimental results. The viscose damping coefficient, VCD, is implemented in LS-DYNA to damp out the contact oscillations. Using the default value of zero for VDC results in instability of the analysis. LS-DYNA recommends using VDC of 40% to 60% of the critical damping to improve stability. The effect of different values of VCD (20%, 40% & 60%) on the wall displacement was evaluated and VDC of 40% was selected which resulted in reasonable responses.

4-3 Comparison of Finite element and experimental results:

In order to validate the numerical simulation of GRS bridge abutment using LSDYNA, the results of numerical simulation is compared with measured data of the full scale shake table test of GRS abutment experiment. The compared results include lateral displacement and acceleration response of wall facing.

4-3-1 Acceleration Response Comparison:

The measured and calculated acceleration history of GRS wall facing for tests 1 and 2 are presented in Figures 4-8 and 4-9. Both analytical and experimental results show acceleration amplification that increases from the base to the top of the wall.

4-3-2 Lateral displacement of wall facing

The calculated and measured displacement histories of the GRS wall facing for Tests 1 and 2 at several points located on the modular concrete blocks are presented in Figures 4-10 and 4-11. The maximum and minimum lateral displacements happen at the top and base of the wall respectively. The lateral displacement increases with increasing the seismic load. Reasonable agreement between the measured and calculated values is noted in Figures 4-10 and 4-11. Most notable is the capability of the finite element simulation of capturing the essence of the two tests--The displacements of the bridge and the sill are very significant in Test 1 while the applied base acceleration is small (0.17 g), whereas the displacements of the bridge and the sill are very small even though the base acceleration was doubled (0.3 g).

4-3-3 Lateral and vertical Displacement of the sill and bridge

The comparison between the calculated and measured displacement histories of the sill's front edge and the bridge edge for tests 1 and 2 are presented in figure 4-12. It's notable that the lateral displacements of the bridge and sill are very significant in test 1, while the applied base acceleration is small (0.17 g), whereas the displacements of the bridge and the sill are very small even though the base acceleration was doubled (0.3 g).

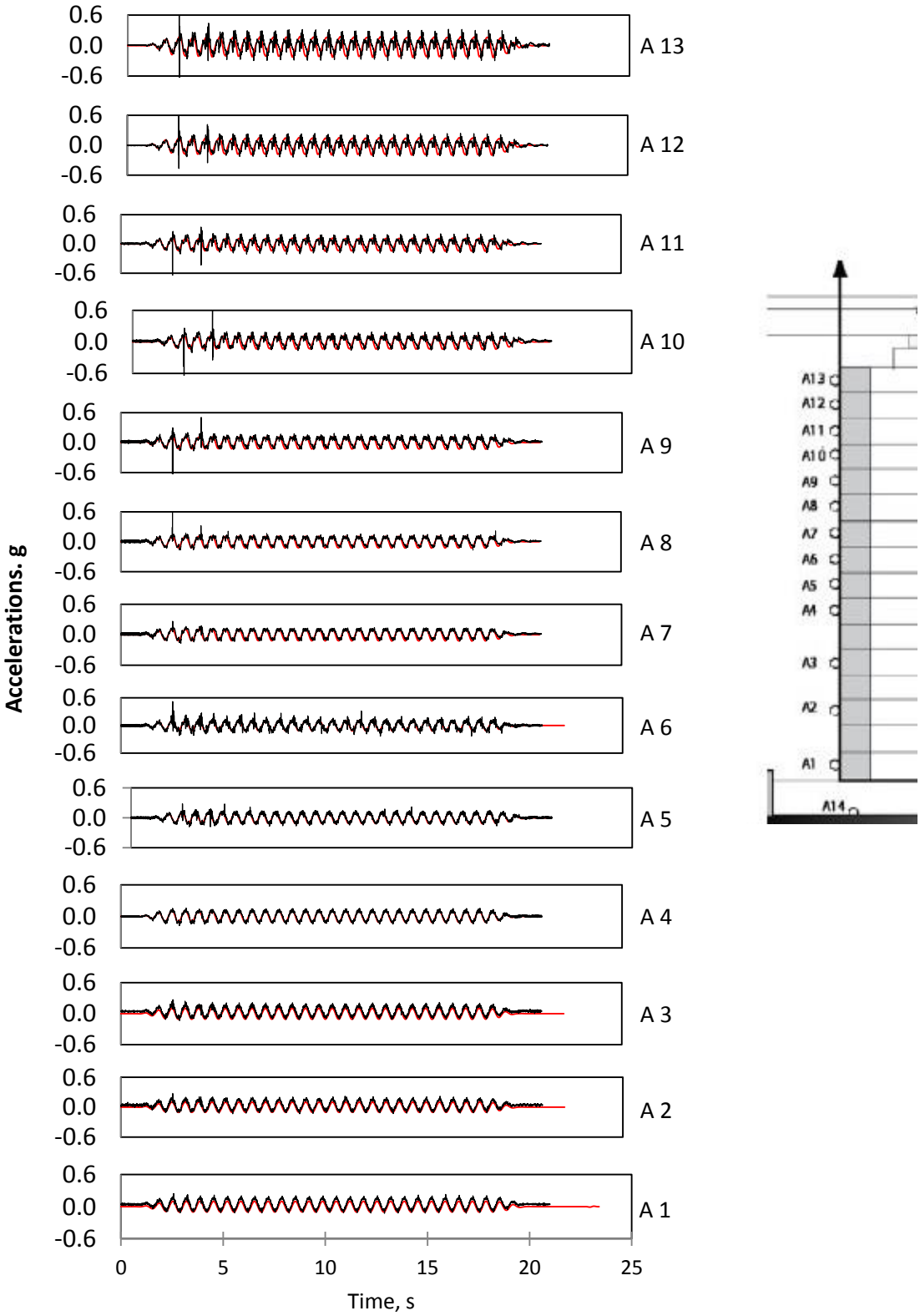

Figure 4-8: Measured (black) and Calculated (red) Acceleration History of GRS Wall Facing (Test 1)

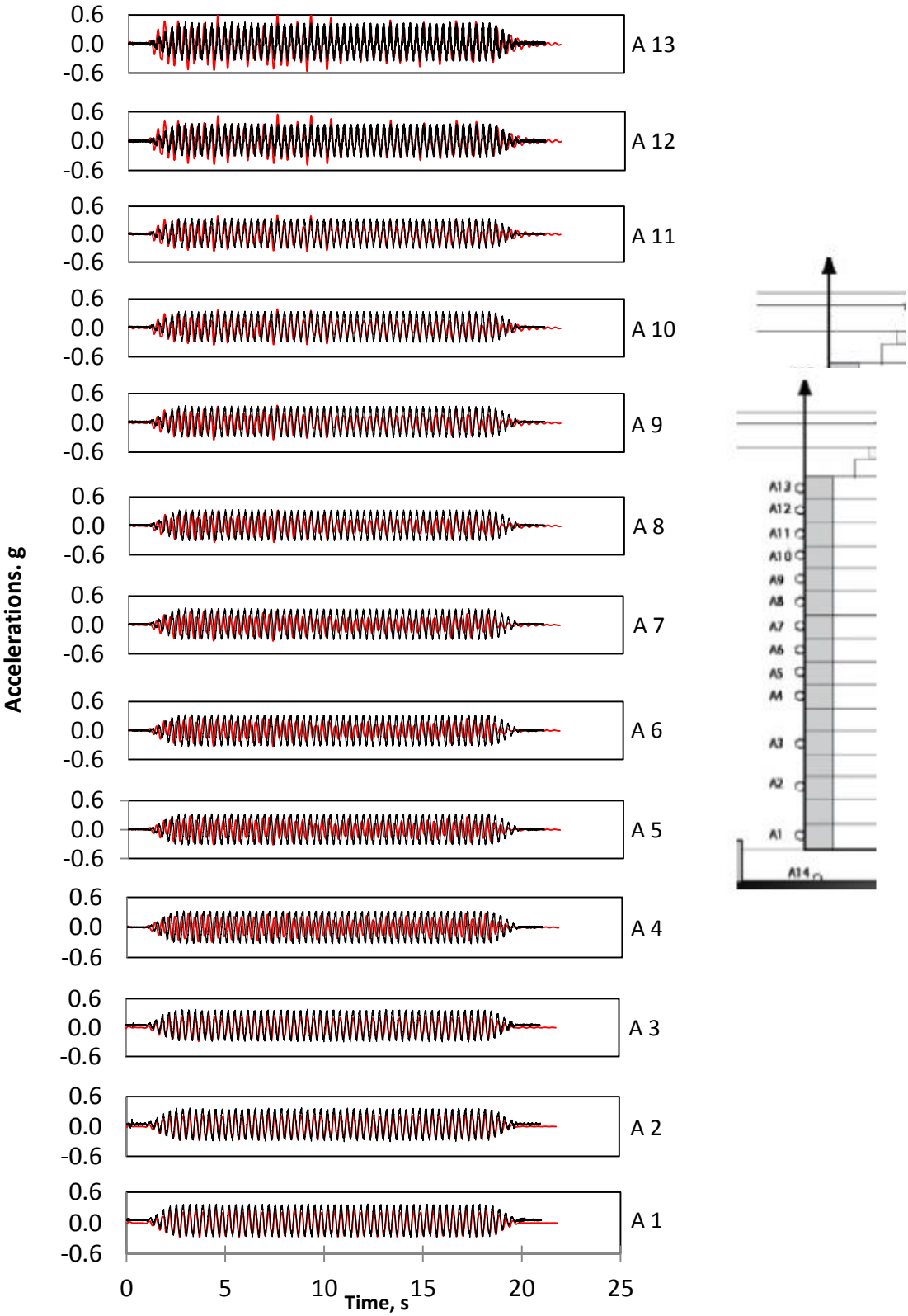

Figure 4-9: Measured (black) and Calculated (red) Acceleration History of GRS Wall Facing (Test 2)

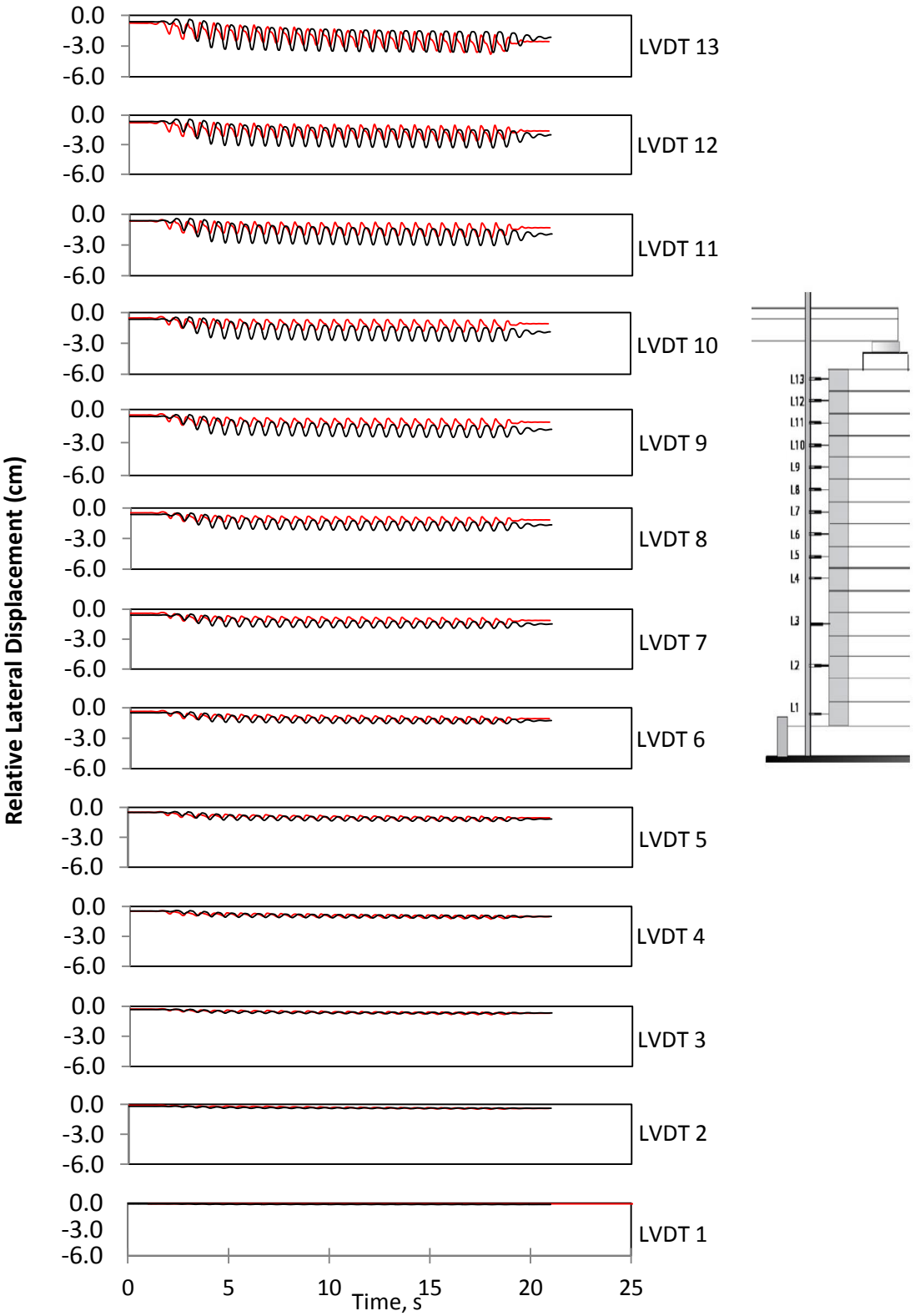

Figure 4-10: Measured (black) and Calculated (red) Displacement History of GRS Wall Facing (Test 1)

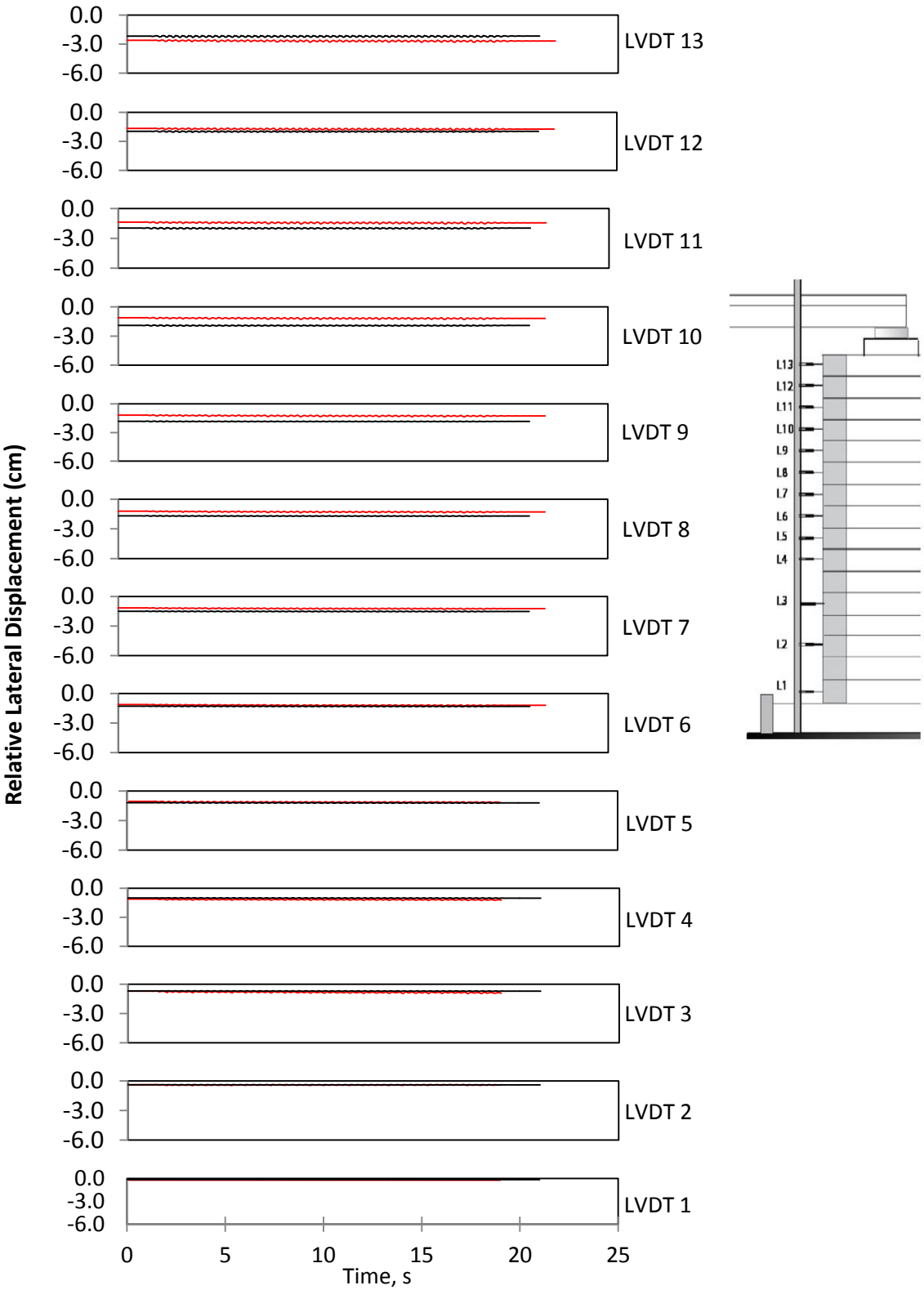

Figure 4-11: Measured (black) and Calculated (red) Displacement History of GRS Wall Facing (Test 2)

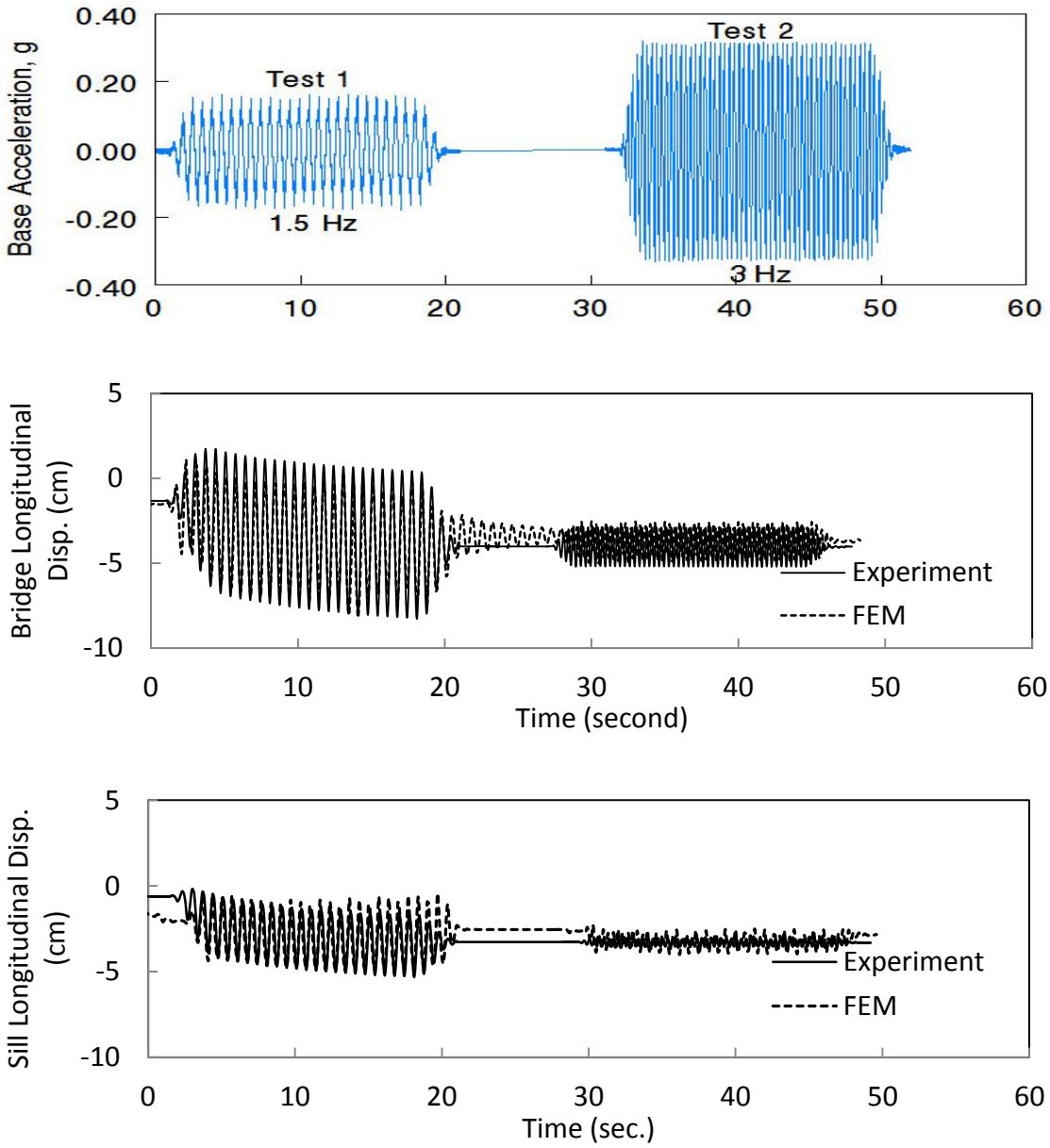

Figure 4-12: Measured and Calculated Bridge and Sill Responses in Tests 1 and 2

Chapter 5: PARAMETRIC ANALYSIS

5-1 Base Case Geometry, Material Properties, and Loading

After the finite element code, LSDYNA, was satisfactorily verified, a parametric study was conducted to investigate seismic performance characteristics of GRS bridge abutments. The performance characteristics as affected by soil placement condition, bridge height (clearance), reinforcement stiffness, reinforcement spacing, and earthquake history were investigated.

The present parametric analysis included three backfill soil types (φ'=34°, 37°, and 40°), two earthquake motions (Kobe 1995 and Northridge 1994), three abutment heights (3 m, 4 m and 5 m), two geotextile stiffness (350 kN/m and 700 kN/m), and three geotextile spacing (20 cm, 40 cm and 60 cm). In total there were 36 combinations in this parametric study.

When analyzing the results, the following parameters were emphasized: the maximum and permanent lateral displacement of the GRS abutment wall, the maximum and permanent lateral displacement of the bridge, the maximum and permanent lateral displacement of the sill, displacement of the sill relative to facing and the maximum acceleration of the GRS abutment wall and the bridge.

The “Base Case” geometry used in the parametric analysis is the same as the GRS abutment used in shake table test. The abutment is 3 m long, 3 m deep, the bridge height (clearance) is 3 m and total abutment height is 3.6 m. The concrete block dimensions are 20 cm × 20 cm ×40 cm. Soil

friction angle for the base case is 40 degree and Geotextile stiffness is 700 KN/m and their spacing is 20 cm. The dimensions and parameters of the base case are kept constant for all cases of the parametric study unless otherwise stated. All finite element models were subjected to gravity loads applied to all model parts and kept constant throughout the analyses. The seismic loading for the base case consisted of horizontal acceleration history of the Kobe 1995 earthquake which is applied at the base of the model.

5-2 Description of Parameters Analyzed

5-2-1 Earthquake Histories

Two earthquake histories are considered in the present parametric analysis: Kobe 1995 (6.9 Magnitude) and Northridge 1994 (6.7 Magnitude). In all analysis only the horizontal component of the earthquake is applied in the longitudinal direction of the bridge.

The near field horizontal acceleration history of Kobe 1995 earthquake (Takarazuka Station) is used for the base case analysis and several other cases of this parametric study (Source: CUE, Conference on the Usage of Earthquake). The peak ground acceleration of this earthquake is 0.694g. The bracketed duration of the earthquake is 12 seconds at acceleration level of 0.05 g. Figure 5-1 (a) shows the acceleration, velocity, and displacement histories of the earthquake.
The acceleration history in Figure 5-1 (a) is applied to the base of the finite element model without scaling. Figure 5-1 (b) shows the acceleration, velocity, and displacement spectra of the earthquake (5% damping).

Another earthquake, the Northridge 1994 earthquake, is used in the analysis of several cases. The near field horizontal acceleration (75 Sylmar-Converter Station East) used herein has a peak ground acceleration of 0.828g (Source: DWP, Los Angeles Department of Water and Power). Its bracketed duration is 20 seconds at acceleration level of 0.05g. Northridge 1994 acceleration, velocity, and displacement histories are shown in Figure 5-2 (a). Figure 5-2 (b) shows the acceleration, velocity, and displacement spectra of Northridge earthquake (5% damping). No scaling was applied to the acceleration history used in the finite element analysis. The Northridge earthquake has a significantly greater peak ground acceleration than the Kobe earthquake. Its duration is substantially longer than that of Kobe earthquake.

5-2-2 Backfill Soil Type

Three backfill soils with internal friction angles of 34º, 37º, and 40º and relative compactions of RC = 90%, 95%, and 100% (ASTM D698), respectively, are used in the analysis to investigate the effects of backfill soil type on the seismic performance of the GRS abutment. The soil parameters used in the analysis were deduced from triaxial tests results conducted on numerous backfill materials (Duncan et al., 1980). Figure 5-3 shows the deviatoric stress-axial strain behavior and the volumetric strain-axial strain behavior of the three soil samples. All three soil types, used in the parametric analysis, were modeled using finite element program LS-DYNA. The FEM results are compared with experimental results in figure 5-4. The material parameters used to describe the soil behavior using Geological Cap Model and generate the curves in Figure 5-4 are shown in table 5-1.

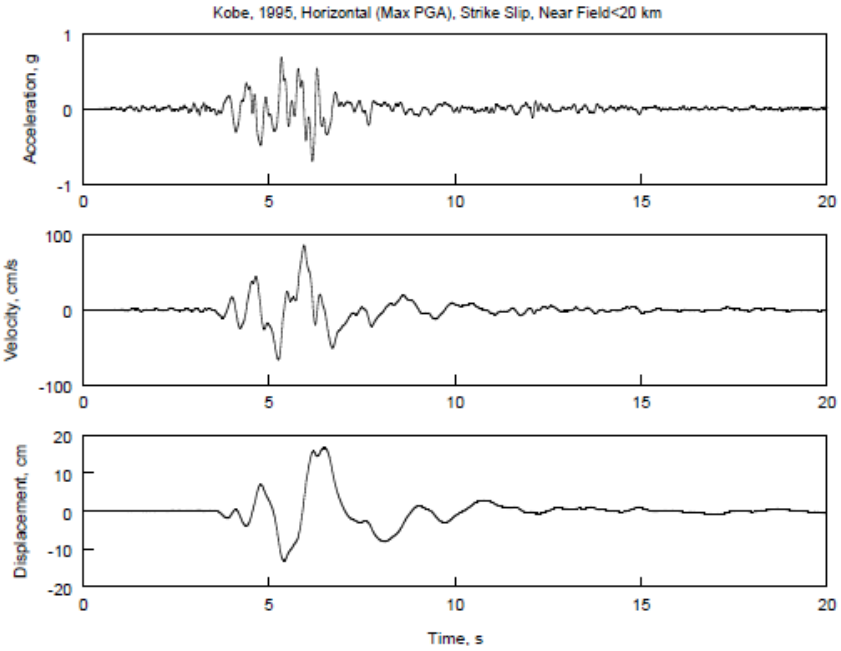

Figure 5-1(a) Acceleration, Velocity, and Displacement History of Kobe 1995 Earthquake

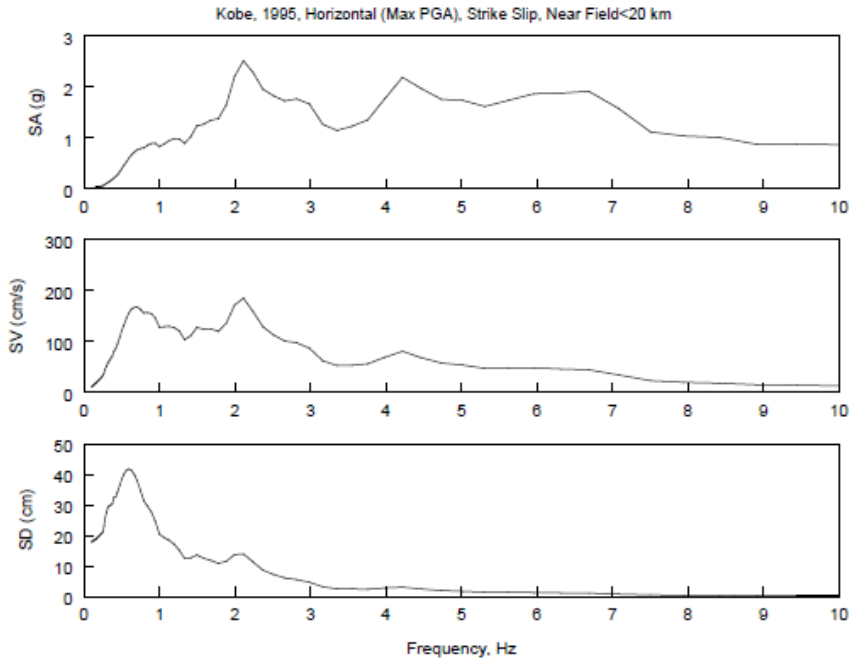

Figure 5-1(b) Response Spectra of Kobe 1995 Earthquake

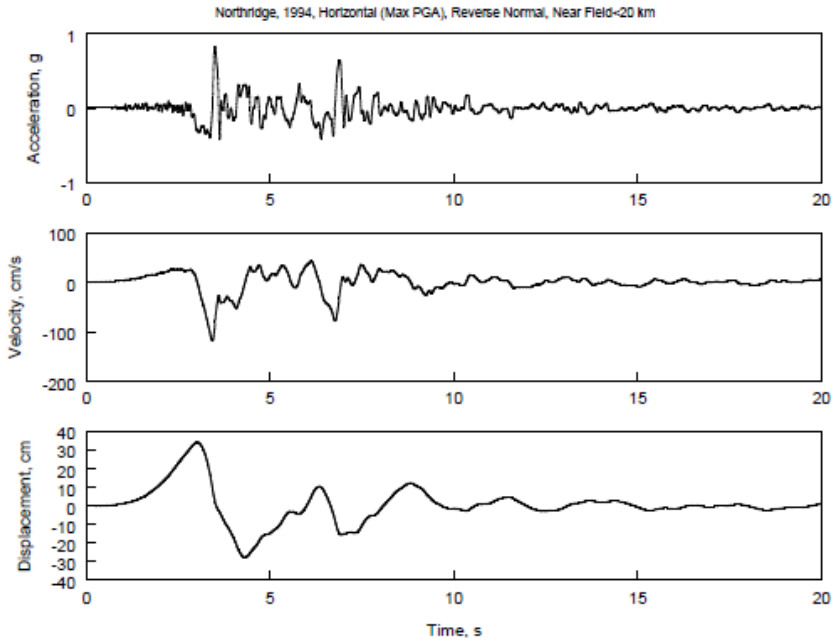

Figure 5-2 (a) Acceleration, Velocity, and Displacement History of Northridge 1994 Earthquake

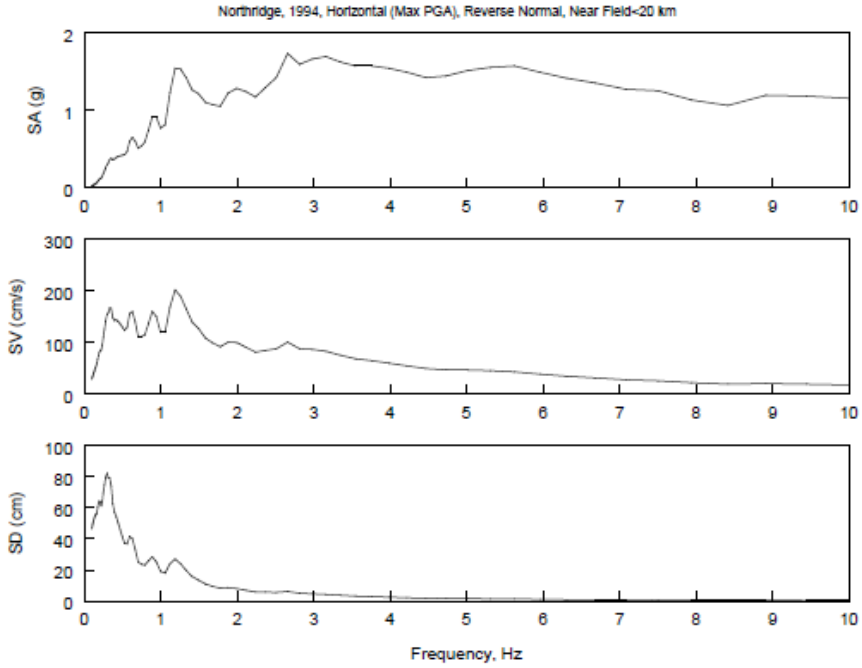

Figure 5-2 (b) Acceleration, Velocity, and Displacement History of Northridge 1994 Earthquake

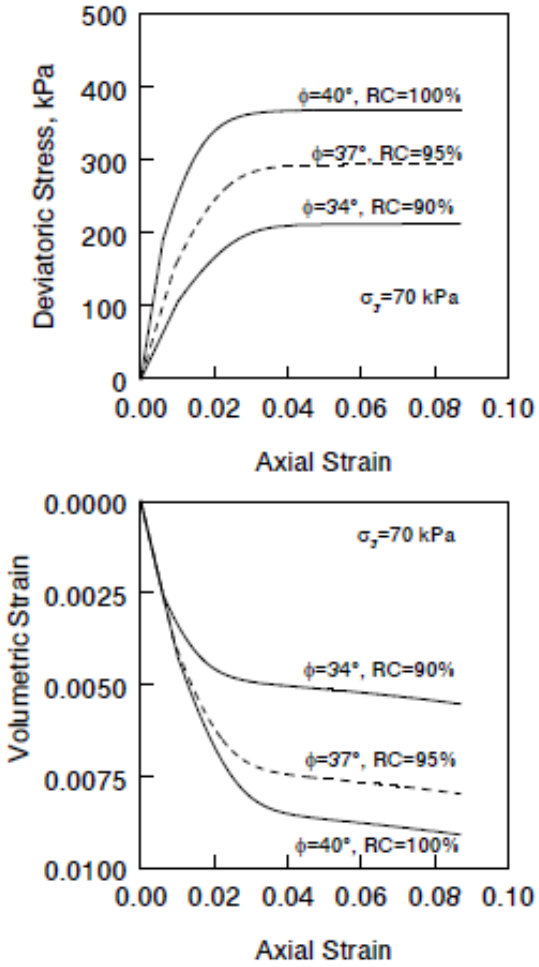

Figure 5-3 Assumed Behavior of Backfill Soils Used in the Parametric Analysis

The study by Duncan et al (1980) presented estimates of stress-strain-strength parameters and volumetric strain-axial strain parameters for various soil types and degrees of compaction. These estimates were made using the compilations of data taken from 135 different soil parameters. Using these data, conservative parameter values have been interpreted for the soils under various types and degrees of compaction. The values of stress-strain-strength parameters and volumetric strain-axial strain parameters of 16 materials averaged from the aforementioned 135 materials were presented in the study. These parameters are called conservative in the sense that they are typical of the lower values of strength and modulus, and the higher values of unit weight for each soil type.

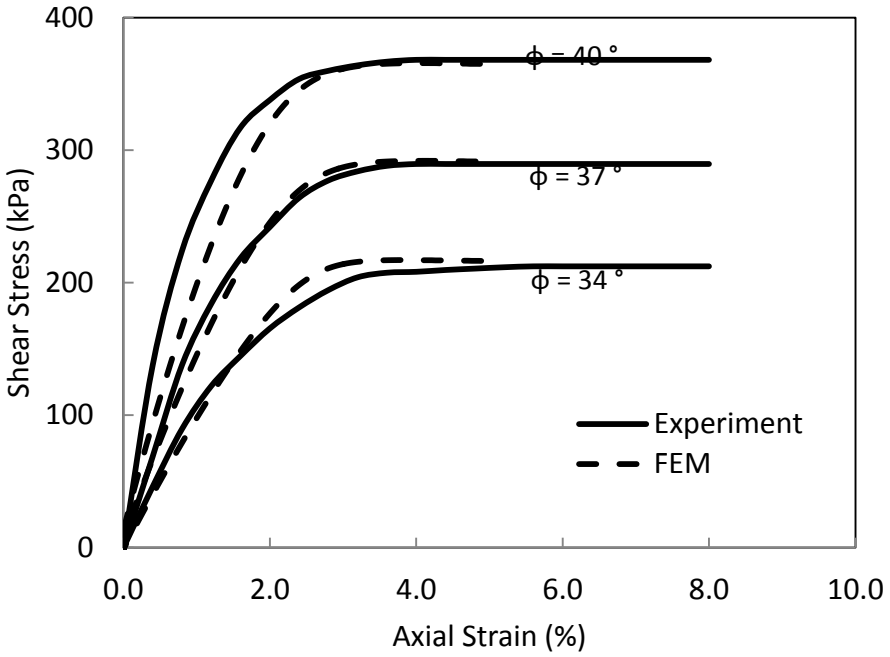

Figure 5-4: The shear stress-axial strain behavior of soils used in the parametric analysis, obtained from experiment and finite element modeling

5-3 Results of the parametric study

The results of parametric study are presented in this section. These results include the effect of soil friction angle, geotextile stiffness, geotextile spacing, abutment height and earthquake history on the seismic performance of the GRS bridge abutment. The FEM models are subjected to two earthquake histories of Kobe 1995 and Northridge 1994. In both cases, only the horizontal component of the earthquake is applied to the base of the finite element model. The acceleration and displacement response of the model GRS abutments are presented in the following sections.

The parametric analysis results described below show that the GRS abutment is highly resistant to such destructive earthquakes. Different combinations of variables used in parametric study are shown in Table 5-2.

Table 5-1: Model parameters for backfill soils used in the parametric study

Parameter	**Unit**	**Φ = 34°**	**Φ = 37°**	**Φ = 40°**
$K°$	psi	1800	2500	3750
G	psi	830	1250	1731
v	-	0.3	0.3	0.3
α	psi	2	3.6	4.6
θ	-	0.265	0.29	0.315
γ	psi	0	0	0
β	1/psi	0	0	0
D	1/psi	0.004	0.0035	0.0030
W	-	0.02	0.02	0.02
R	-	2	2	2
X_o	psi	0	0	0
C		2000	2000	2000
N		4.9	4.9	4.9

Table 5-2: Different combinations used in the parametric study

Soil friction angle, (degree)	bridge clearance (Height) (m)	Geosynthetic stiffness (KN/m)	Earthquake	geosynthetic Spacing (cm)
34	3	700	Kobe	20
37	3	700	Kobe	20
40	3	700	Kobe	20
34	3	700	Northridge	20
37	3	700	Northridge	20
40	3	700	Northridge	20
34	3	350	Kobe	20
37	3	350	Kobe	20
40	3	350	Kobe	20
34	3	350	Northridge	20
37	3	350	Northridge	20
40	3	350	Northridge	20
34	3	700	Kobe	40
37	3	700	Kobe	40
40	3	700	Kobe	40
34	3	700	Kobe	60
37	3	700	Kobe	60
40	3	700	Kobe	60
34	3	700	Northridge	40
37	3	700	Northridge	40
40	3	700	Northridge	40
34	3	700	Northridge	60
37	3	700	Northridge	60
40	3	700	Northridge	60
34	4	700	Kobe	20
37	4	700	Kobe	20
40	4	700	Kobe	20
34	4	700	Northridge	20
37	4	700	Northridge	20
40	4	700	Northridge	20
34	5	700	Kobe	20
37	5	700	Kobe	20
40	5	700	Kobe	20
34	5	700	Northridge	20
37	5	700	Northridge	20
40	5	700	Northridge	20

5-3-1 Effects of Soil Friction Angle

To study the effects of soil friction angle on the seismic performance of GRS abutments, three different backfill soils with the internal friction angles of 34º, 37º, 40º were considered in parametric analysis. In all three cases the GRS abutment is 10 ft high. Two earthquake histories of Kobe and Northridge are used as input motion. The seismic performances of maximum and permanent lateral displacement of the facing, sill and bridge, the acceleration of the facing and bridge, and displacement of the sill relative to the facing when the abutment is subjected to earthquake histories of Kobe and Northridge are presented in Figure 5-5 and 5-6.

Figure5-5 presents the results of the parametric analysis for a GRS abutment with different backfill soils (internal friction angle: 34º, 37º, 40º) subjected to Kobe earthquake. In general, the performance of the GRS abutment is very favorable for the three backfill soil types. From Figure 5-5(a), the maximum permanent displacement of approximately 91 mm (3.6 in.) occurred at the top of the lower GRS wall with backfill soil having an internal friction angle of 34º. The maximum acceleration of the facing also occurred at the top of the GRS wall (Figure 5-5(c)). The acceleration for the backfill soil having an internal friction angle of 34º is approximately 0.94 g (362 in./s^2). The maximum acceleration increased with increasing the internal friction angle as shown in Figure 5-5(c). This may seem counterintuitive. However, when the stiffness of any part of the model is changed, especially the backfill soil that possess the largest mass in the model, the natural frequency of the entire model will change. This change in model natural frequency will change the model dynamic response based on the acceleration spectra of Kobe

earthquake shown in Figure 5-1(b). Note that the backfill soil with a higher internal friction angle has a greater initial elastic modulus (i.e., greater initial stiffness).

Figure 5-5(e) presents the maximum and the permanent displacements of the sill. These displacements are greatly affected by the mass of the bridge and the characteristics of the elastomeric pad used in the analysis. The permanent displacements of the sill is about 100 mm (4 in.) as shown in the figure 5-5(e).

Figure 5-5(f) presents the sill clearance (the distance between the edge of the sill and the back of the facing block) at maximum displacement of the facing and the sill. The figure indicates that the clearance remained nearly unchanged even at maximum ground shaking.

Figure 5-5(b) shows the bridge maximum and permanent displacements. These displacements are also greatly affected by the mass of the bridge and the characteristics of the elastomeric pads used in the analysis. The permanent displacements of the bridge is approximately 4 in. (100 mm) for the backfill soil having an internal friction angle of 34º as shown in the figure 5-5(b).

Figure 5-5(d) presents the maximum acceleration of the bridge deck. The maximum acceleration of the bride deck (approximately 1.05 g) is not greatly affected by the soil friction angle and seems to be independent of the backfill soil type. This can be attributed to the use of the elastomeric pads.

The Northridge earthquake is substantially larger than Kobe earthquake in terms of peak ground acceleration and duration. When subjected to Northridge earthquake, the GRS abutment sustained the permanent lateral displacements up to 140 mm (5.5 in.). The displacements slightly decreased with increasing the backfill strength and stiffness as shown in Figure 5-6(a). The same observation applies to the displacement of the sill and the bridge as shown in Figures 5-6(e) and 5-6(b), respectively. The GRS wall and the bridge both suffered significant accelerations as shown in Figures 5-6(c) and 5-6(d), respectively.

Figure 5-13 shows the displacement histories of one point on the bridge and three points on the top, middle and bottom of the GRS abutment wall facing.

5-3-2 Effects of Abutment Height

To study the effects of bridge height on the seismic performance of GRS abutments, three different bridge heights of H=3 m, 4 m and 5 m were considered in parametric analysis. The effect of bridge height is also studied with different backfill soils with friction angles of 34º, 37º, 40º. Two earthquake histories of Kobe and Northridge are used as input motion for all cases. In all cases, the geotextile stiffness is 700 KN/m. The seismic performances of maximum and permanent lateral displacement of the facing, sill and bridge and accelerations of the facing and bridge are presented in Figures 5-7 and 5-8.

Figure 5-7 indicates that the lateral displacement of the GRS bridge abutment increases with the increase of the height of the abutment. Better compacted backfill soils showed slight improvement in term of lateral displacements. When subjected to Kobe earthquake, the GRS

abutment with the height of 5 m, suffered permanent lateral displacement of approximately 13 cm for the less compacted backfill. Better compacted backfill soils showed slight improvement in term of lateral displacement. The analysis also showed that the GRS facing experienced accelerations exceeding 1.1g.

When subjected to Northridge earthquake, the GRS abutment with the height of 5 m suffered significant maximum lateral displacements approaching 22 cm. The maximum displacements decreased with increasing the backfill strength and stiffness as shown in Figure 5-8(a). The same observation applies to the displacement of the bridge as shown in Figure 5-8(b). The GRS wall and the bridge both suffered significant accelerations as shown in Figures 5-8(c) and 5-8(d), respectively.

Although Kobe earthquake and Northridge earthquake have nearly the same magnitudes (6.9 and 6.7, respectively), they differ in their peak ground accelerations (0.694g and 0.828g, respectively) and in their durations (10.88 s and 17.06 s, respectively). Their effects on the GRS abutment-bridge system are very different. The lateral displacements of the GRS wall caused by Northridge earthquake was significantly larger than the displacements caused by the Kobe earthquake (Figures 5-7a and 5-8a). On the other hand, both earthquakes caused about the same acceleration of the GRS wall as shown in Figures 5-7d and 5-8d.

5-3-3 Effects of Earthquake History

Although Kobe earthquake and Northridge earthquake have nearly the same magnitudes (6.9 and 6.7, respectively), they differ in their peak ground accelerations (0.694g and 0.828g,

respectively) and in their durations (10.88 s and 17.06 s, respectively). Their effects on the GRS abutment-bridge system are very different. For a low clearance bridge [H1=3 m (10 ft)], the permanent lateral displacement of the GRS wall caused by Kobe earthquake is approximately 91 mm (3.6 in.) (Figure 5-5(a)) for a backfill with an internal friction angle of 34º. In contrast, the Northridge earthquake caused a permanent lateral displacement of 140 mm (5.5 in.) approximately (Figure5-6(a)). Also, Northridge earthquake caused higher acceleration of the GRS wall as shown in Figures 5-5(c) and 5-6(c).

For the case of high bridge clearance [H1=5 m (16 ft)], the permanent lateral displacement of the GRS wall caused by Kobe earthquake (Figure 5-7(a)) is approximately 130 mm (5.5 in.) for a backfill with an internal friction angle of 34º. The Northridge earthquake caused a permanent lateral displacement of 223 mm (8.8 in.) as shown in Figure 5-8(a). The GRS wall acceleration caused by the Northridge earthquake are higher than those caused by Kobe earthquake.

5-3-4 Effects of Geosynthetic Stiffness

To study the effect of geosynthetic stiffness on the seismic behavior of the GRS abutment-bridge system, two geosynthetic stiffnesses of 700KN/m and 350KN/m are considered. Three different soil friction angles and two earthquake histories of Kobe and Northridge are also considered in this evaluation.

Figure 5-9 shows the behavior of the bridge abutment system when the Kobe earthquake is applied and Figure 5-10 shows the behavior of the system with the application of the Northridge earthquake. As the results show, the effect of reducing the geosynthetic stiffness on the seismic behavior of the GRS abutment-bridge system is small. The maximum displacement of the facing and bridge slightly decrease with the increase of the geosynthtic stiffness; implying that the GRS mass behaves as a single coherent composite. The permanent deformation of the wall and bridge increase when the stiffness of the geotextile is reduced. This change is more evident when the northridge earthquake history is applied. Northridge earthquake has a more destructive effect due to its higher acceleration.

5-3-5 Effects of Geosynthetic Spacing

To study the effect of reinforcement spacing on the seismic performance of GRS abutments,, three vertical spacing of 20 cm, 40 cm and 60 cm are evaluated in the parametric study.
In all cases the GRS abutment is 3 m high and the geotextile stiffness is 700 KN/m. Three soil friction angles of 34°, 37° and 40° are considered in the evaluations and two earthquake histories of Kobe and Northridge are used as input motion. The seismic performances of maximum and permanent lateral displacement of the facing, sill and bridge, maximum accelerations of the facing and bridge and displacement of the sill relative to facing are presented in Figures 5-11 and 5-12.

The maximum displacement of the GRS abutment bridge system increase with the increase of the geotextile spacing. Increasing the geotextile spacing from 20 cm (base case) to 40 cm, caused

very little effect on the system during the application of both Kobe and Northridge earthquake as shown in Figures 5-11 and 5.12. But when the geotextile spacing is increased to 60 cm, the maximum displacement of the abutment increases significantly. It should also be noted that 60 cm reinforcement spacing is not recommended since it does not provide enough reinforcement and will not allow to reach desired compaction.

As indicated earlier, the dynamic response of the GRS abutment-bridge system is dominated by the backfill soil characteristics including initial soil stiffness and its hysteretic energy-absorbing cyclic behavior. Using smaller geosynthetic spacing would cause the backfill soil to be better compacted under the same compaction effort (because of the smaller lift thickness). This effect was not accounted for in this parametric analysis. Previous study has revealed that reinforcement spacing has significant effect on compaction induced stresses in the fill. The increase in lateral stresses due to fill compaction at close reinforcement spacing will increase soil stiffness and perhaps its cyclic energy absorption behavior, which were not accounted for in this parametric study. The effects of reinforcement spacing on seismic resistance of GRS abutment should be further investigated

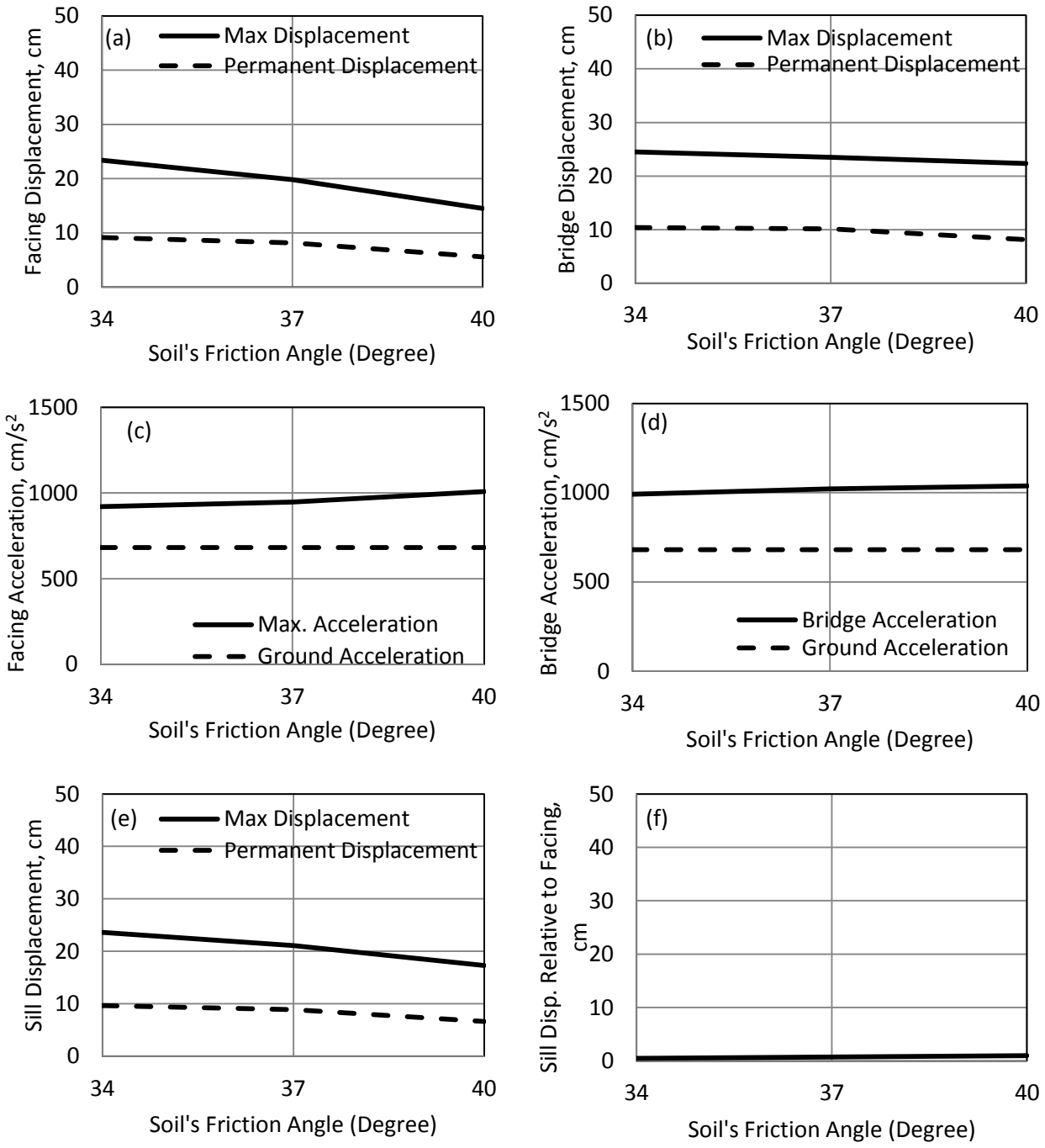

Figure 5-5: Effect of soil friction angle on displacement and acceleration of the facing, bridge and Sill; (Abutment height: 3 m, Geotextile stiffness: 700KN/m, Geotextile spacing: 20 cm, Kobe Earthquake)

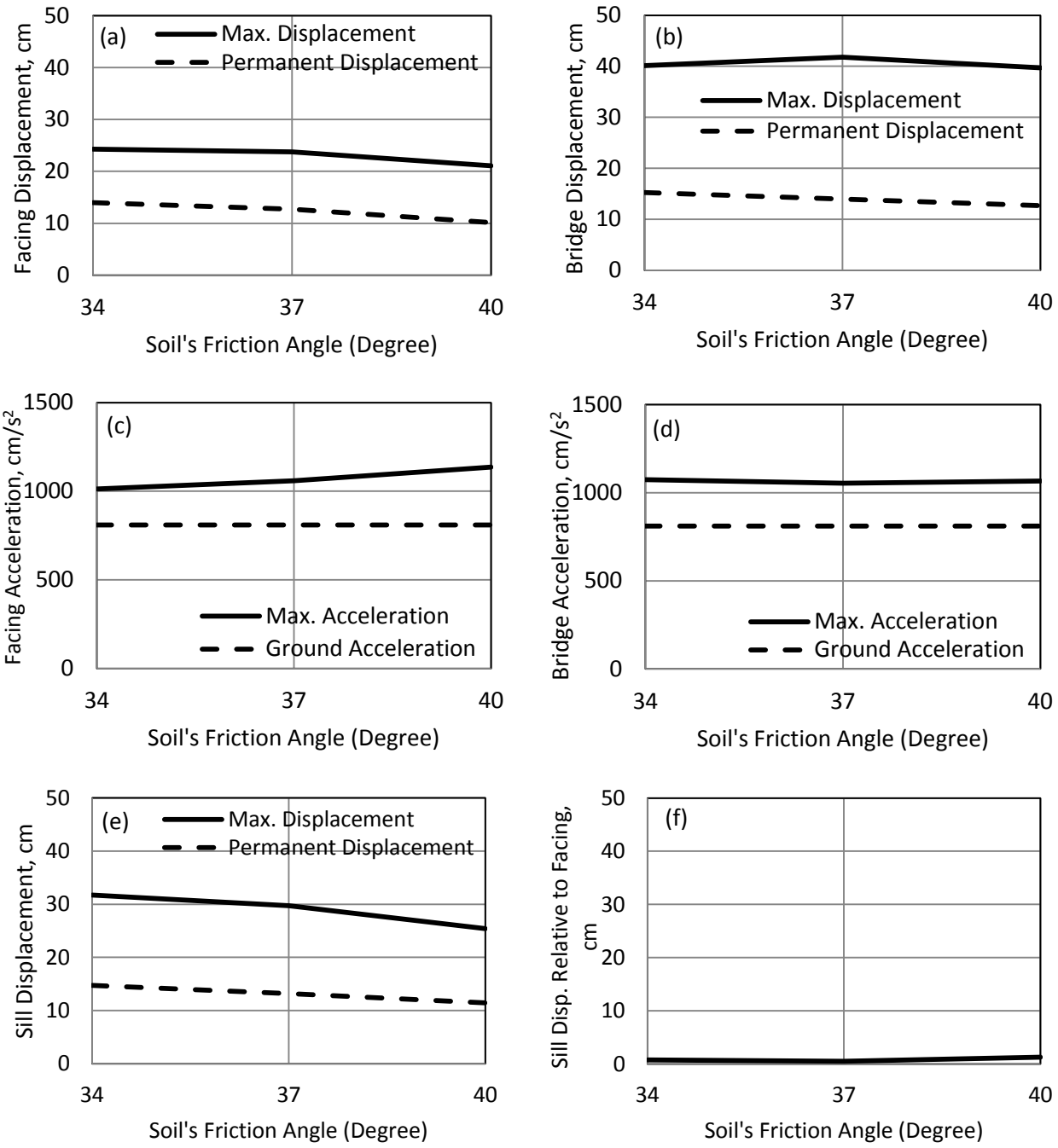

Figure 5-6: Effect of soil friction angle on displacement and acceleration of the facing, bridge and Sill; (Abutment height: 3 m, Geotextile stiffness: 700KN/m, Geotextile spacing: 20 cm, Northridge Earthquake)

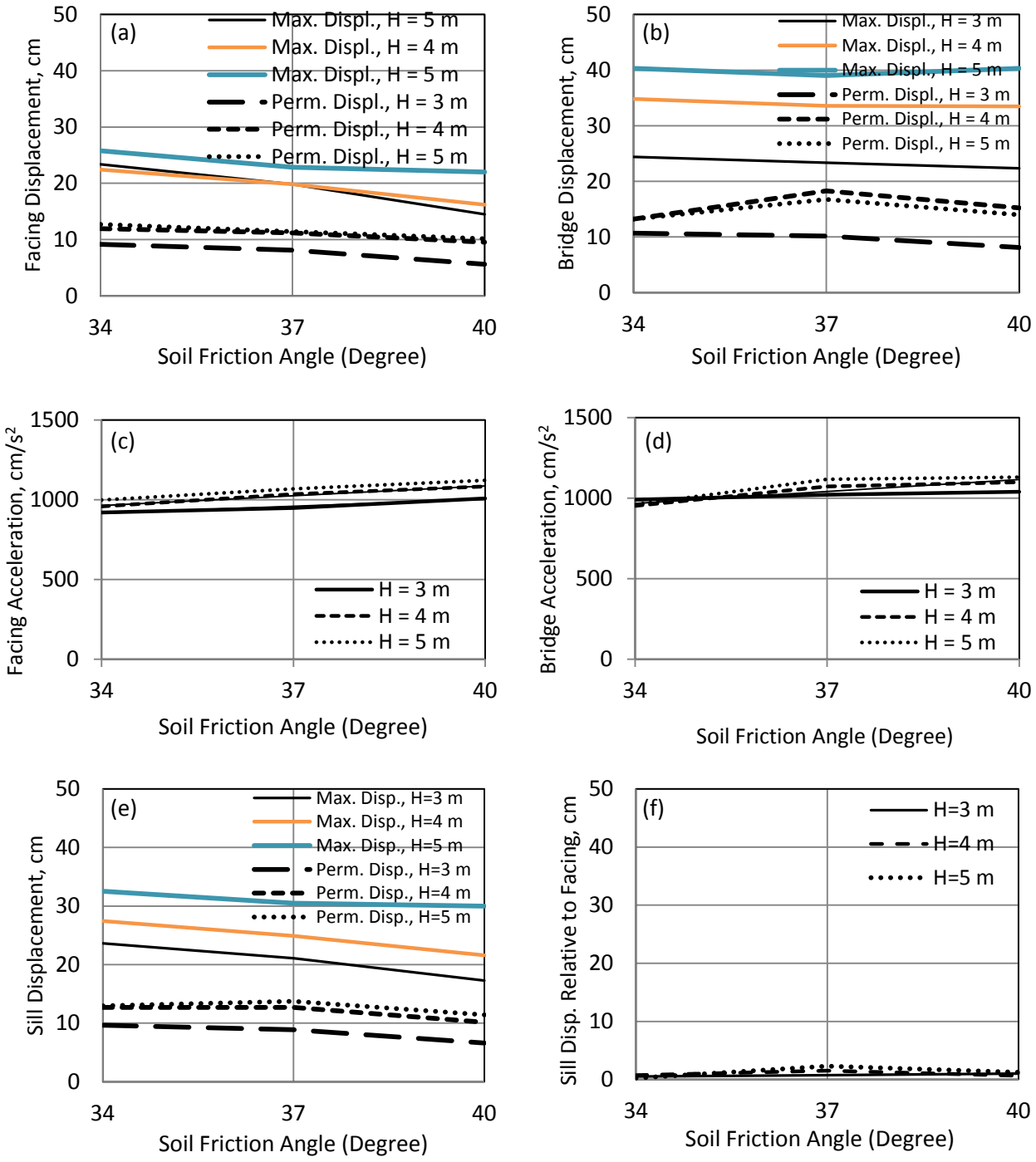

Figure 5-7: Effect of abutment height on displacement and acceleration of the facing, bridge and Sill; (Abutment height: 3 m, 4 m & 5 m, Geotextile stiffness: 700KN/m, Geotextile spacing: 20 cm, Kobe Earthquake)

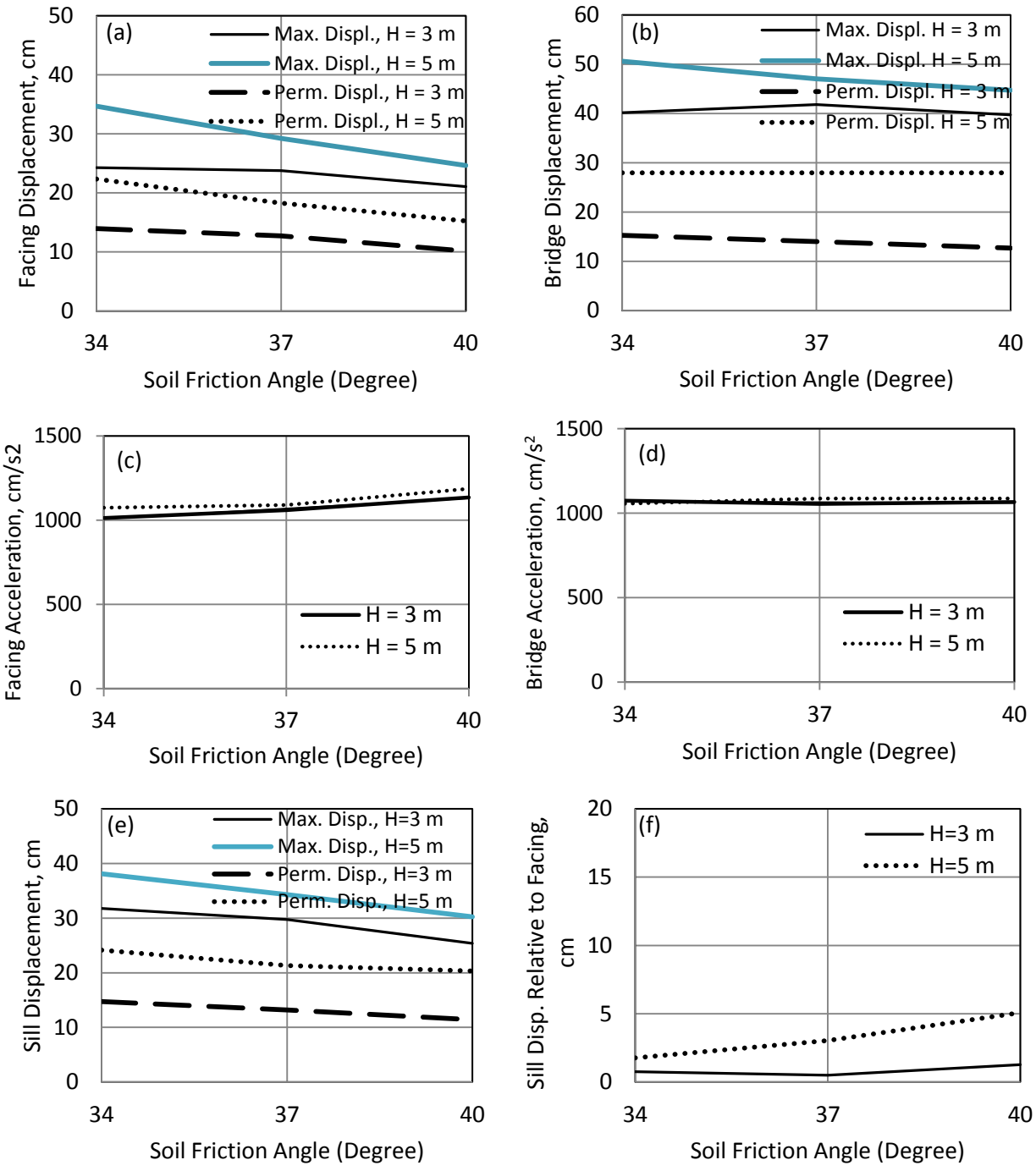

Figure 5-8: Effect of abutment height on displacement and acceleration of the facing, bridge and Sill; (Abutment height: 3 m, 4 m & 5 m, Geotextile stiffness: 700KN/m, Geotextile spacing: 20 cm, Northridge Earthquake)

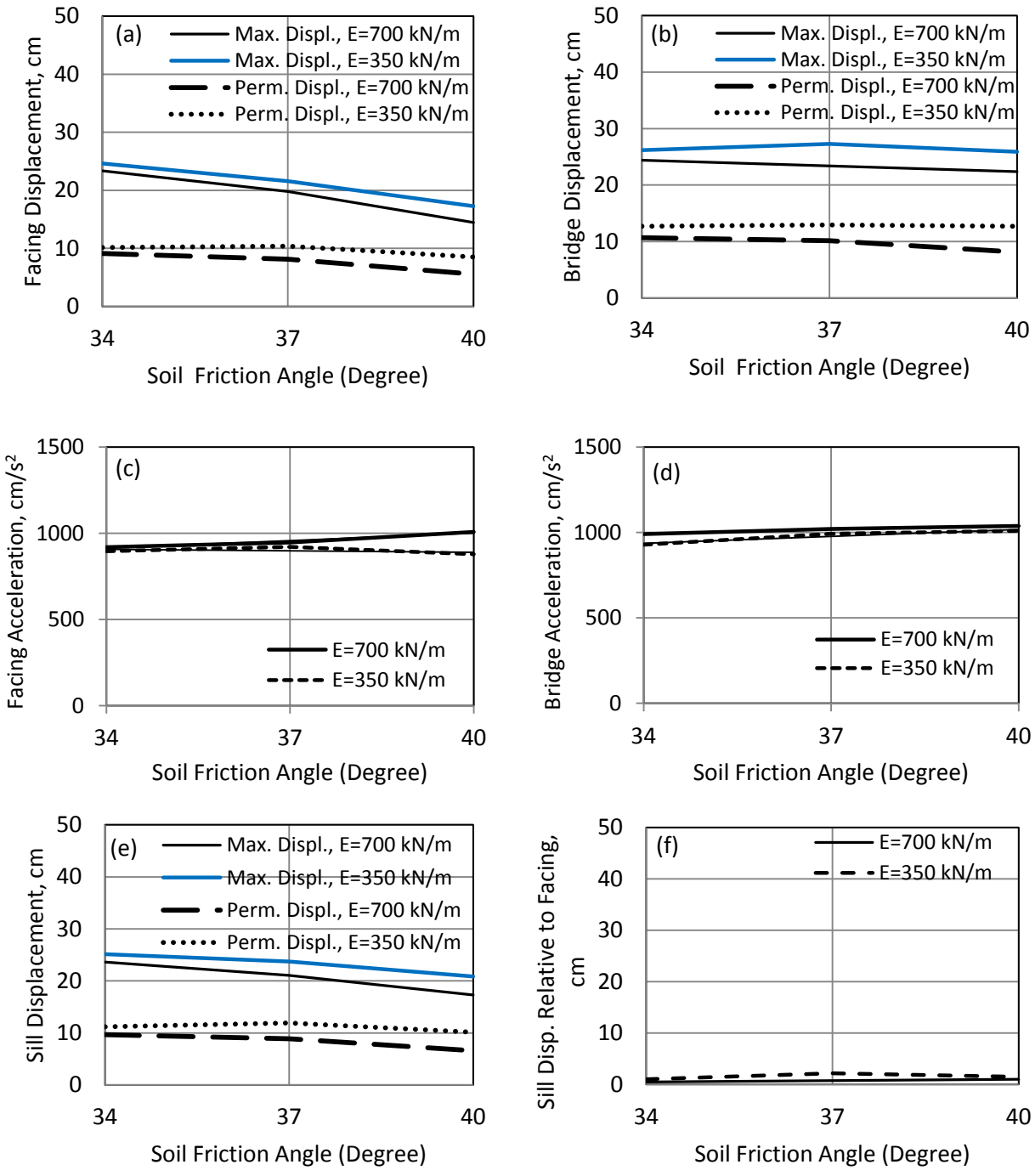

Figure 5-9: Effect of soil geotextile stiffness on displacement and acceleration of the facing, bridge and sill; (Abutment height: 3 m, Geotextile stiffness: 350KN/m and 700KN/m, Geotextile spacing: 20 cm, Kobe Earthquake).

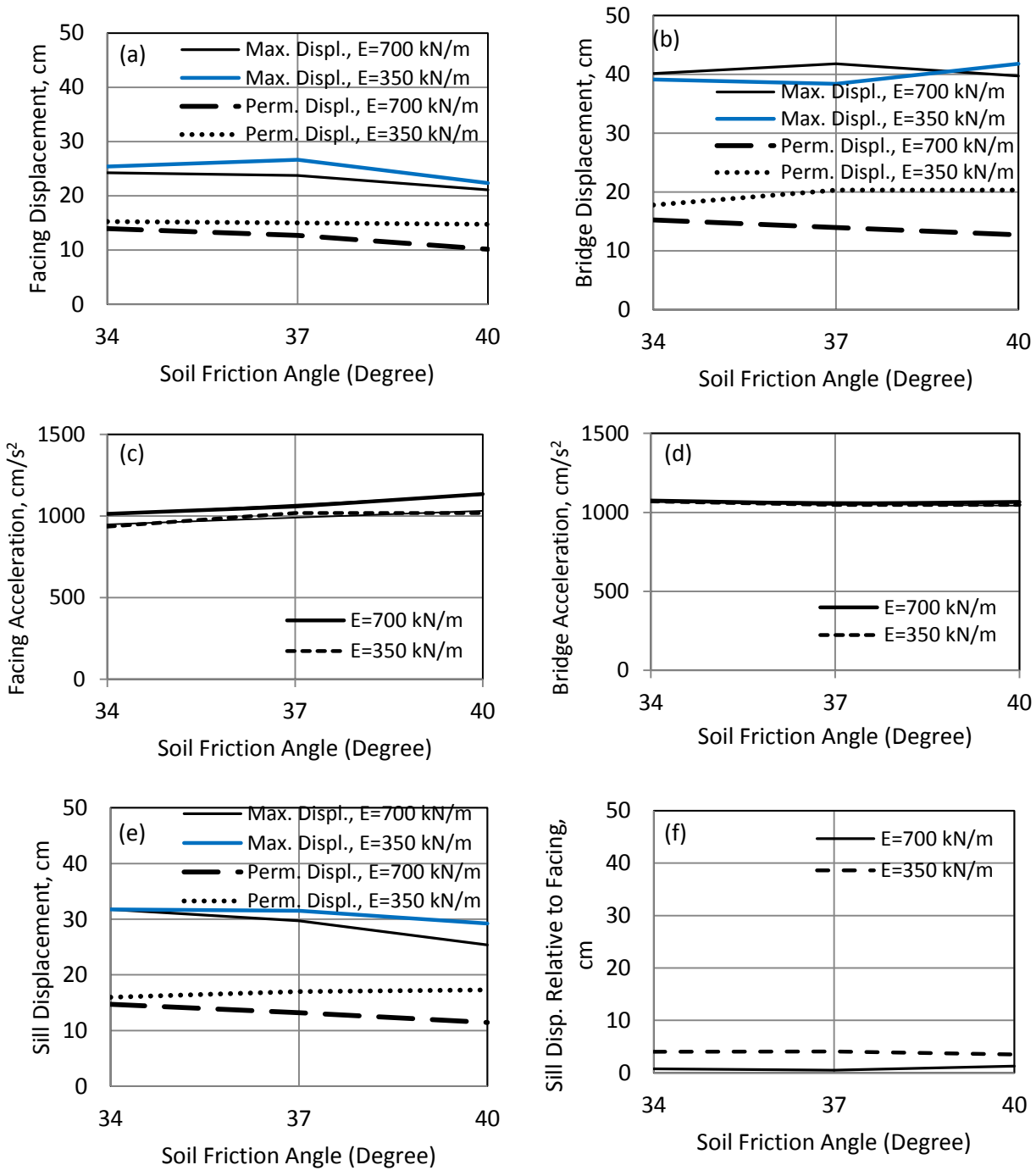

Figure 5-10: Effect of soil geotextile stiffness on displacement and acceleration of the facing, bridge and sill; (Abutment height: 3 m, Geotextile stiffness: 350KN/m and 700KN/m, Geotextile spacing: 20 cm, Northridge Earthquake).

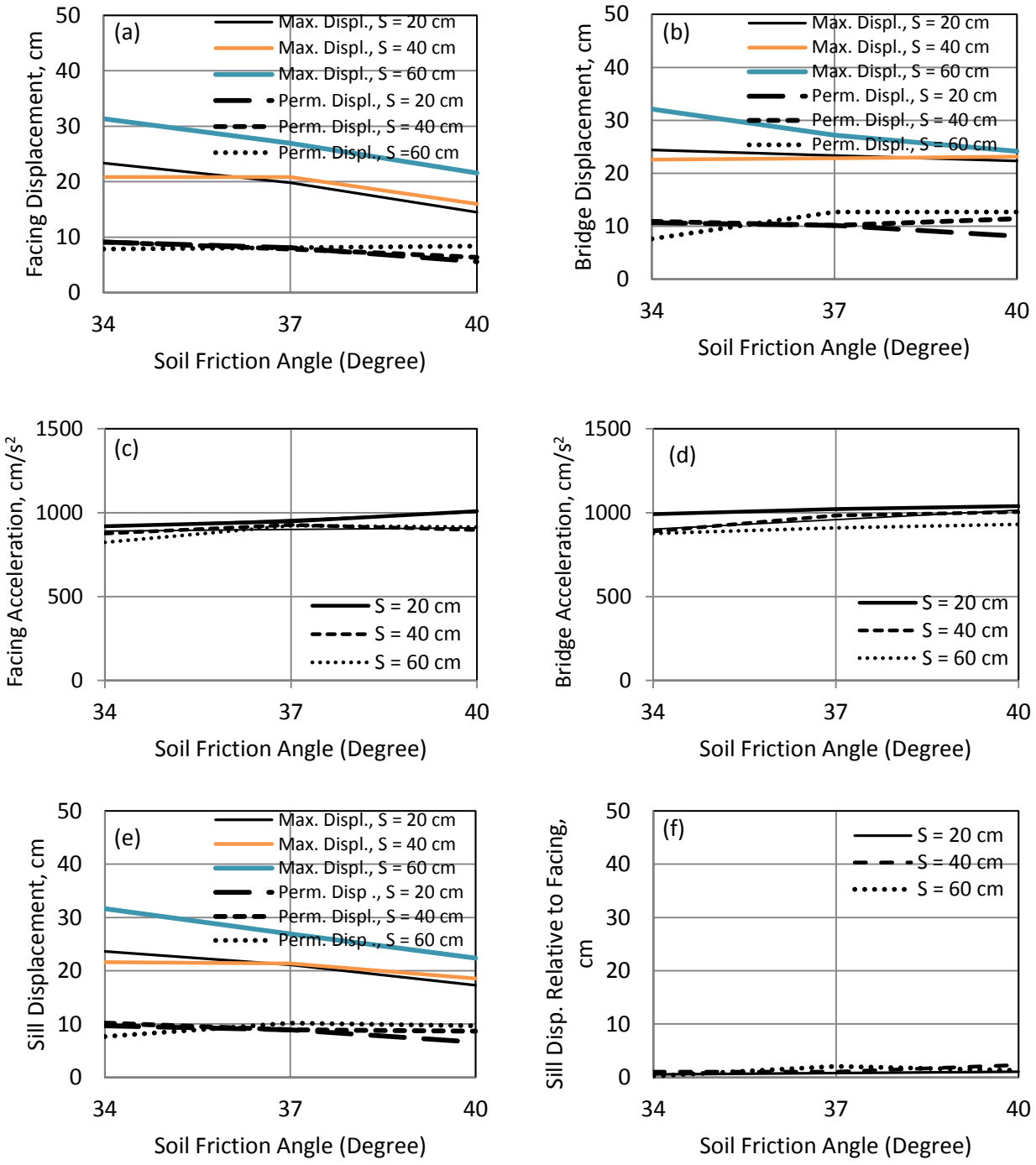

Figure 5-11: Effect of geotextile spacing on displacement and acceleration of the facing, bridge and Sill; (Abutment height: 3 m, Geotextile stiffness: 700KN/m, Geotextile spacing: 20 cm, 40 cm, 60 cm, Kobe Earthquake).

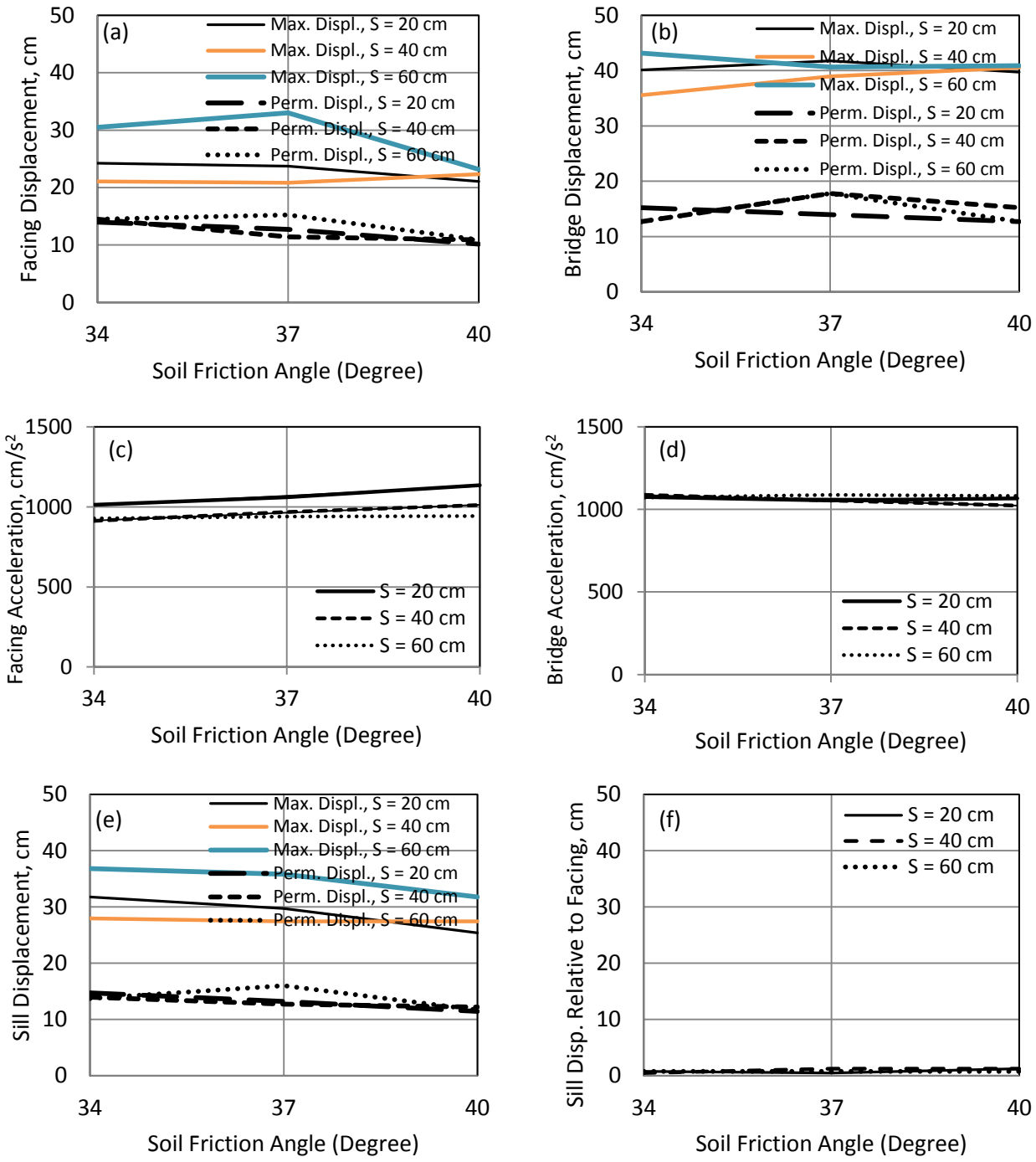

Figure 5-12: Effect of geotextile spacing on displacement and acceleration of the facing, bridge and Sill; (Abutment height: 3 m, Geotextile stiffness: 700KN/m, Geotextile spacing: 20 cm, 40 cm, 60 cm, Northridge Earthquake).

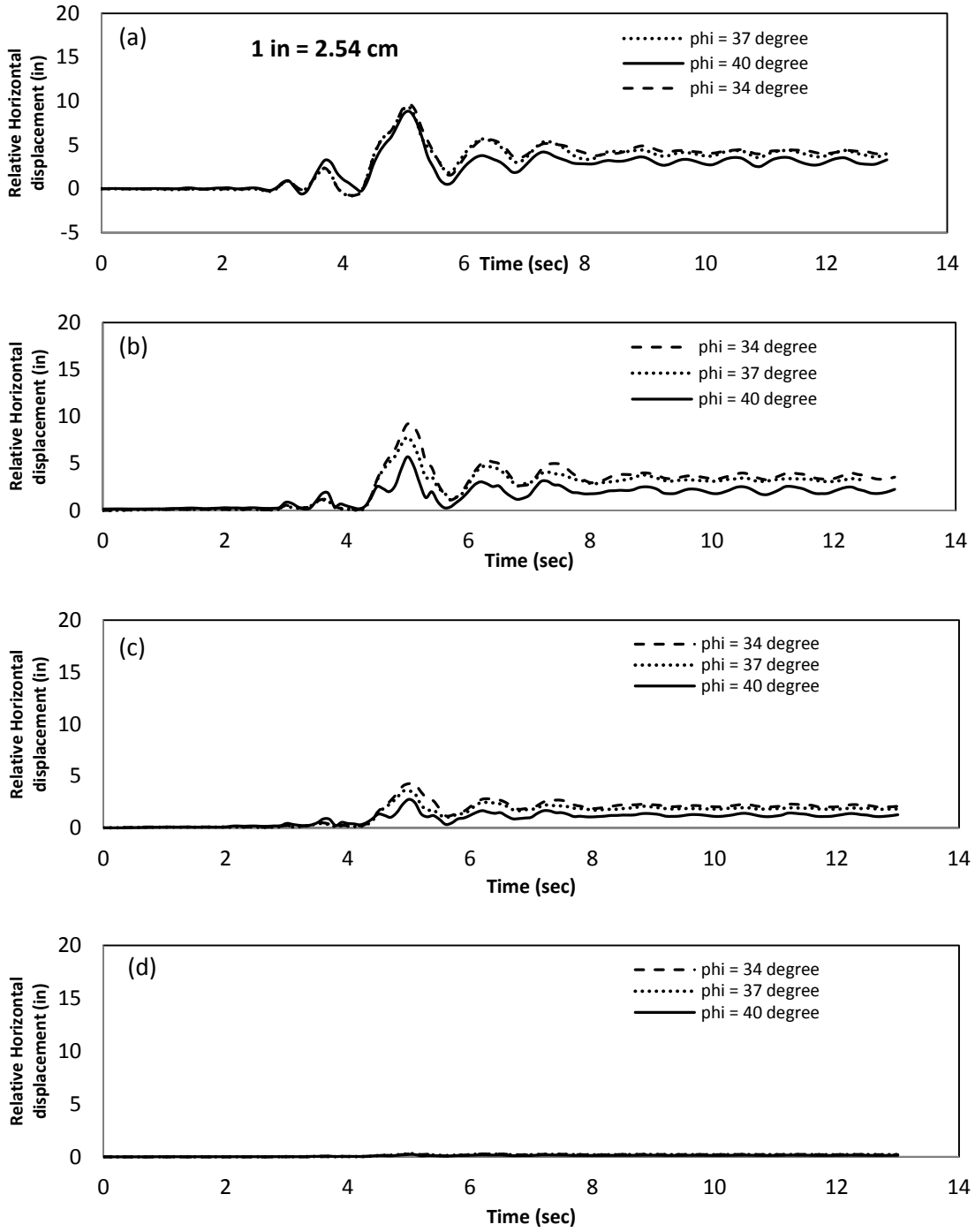

Figure 5-13 Effect of soil friction angle on relative horizontal displacement of the bridge and abutment facing (H=10ft, S=8in, E=700KN/m, Kobe earthquake), (a)bridge, (b)top of the abutment, (c)middle of the abutment, (d)bottom of the abutment.

5-4 Three dimensional bridge system model

In order to study the effect of earthquake direction (both longitudinal and transverse direction), a three dimensional bridge model was created using LS-DYNA. The bridge height is H=4.66 m (15.3 ft) and the bridge span is L=20.0 m (65.6 ft). The model length in the transverse direction is 13.68 m (44.9 ft). The modular block facing consisted of concrete blocks with 200-mm (8 in.) width, 200-mm (8 in.) height, and 400-mm (16 in.) length. The three dimensional model geometry is shown schematically in Figure 5-14. The analytical model is based on the "Geosynthetic Reinforced Soil Integrated Bridge System", proposed and tested by the Federal Highway Administration. Figure 5-15 shows a closer view of the GRS abutment and Figure 5-16 shows the arrangement of geosynthetics in the GRS bridge abutment of the 3D bridge system.

The internal friction angle of the backfill soil for the 3D bridge model was assumed to be 37º. The Parameters used for geotextile and soil are presented in tables 3-5 and 5-1 respectively.

In all analysis cases the length of the finite element mesh behind each abutment is taken as five times the total height of the GRS abutment. This is deemed necessary to reduce the boundary effects on the finite element model of the GRS abutment-bridge system.

The finite element model consist of 341493 elements (Solid and shell) and total of 2608 parts. The contact type Automatic Single Surface-Smooth is selected for this model. The top three rows of facing blocks are tied together via contact type "Tied Surface to Surface", since in practice the top three rows of facing blocks are tied using rebar and mortar. Fully integrated S/R solid element (type -2) are used for soil and facing blocks which is an accurate formulation intended for elements with poor aspect ratio and completely eliminates hour glassing without imposing

unrealistic stiff behavior to the model. The geosynthetics are modeled using default element of Belytschko-Tsay.

The finite element model was subjected to gravity loads applied to all model parts including the bridge. Two earthquake histories of Kobe 1995 (6.9 Magnitude) and Northridge 1994 (6.7 Magnitude) are considered in this section. The horizontal component of the earthquake is applied in either the longitudinal direction or transverse direction of the bridge.

The analyses show that the bridge-abutment system remains stable and the permanent deformations of the GRS abutments are deemed acceptable following destructive earthquakes such as Kobe and Northridge.

Figures 5-17 and 5-18 show the lateral displacement of the facing wall with depth when subjected to Kobe earthquake loading in longitudinal and transverse directions of the bridge. The analyses showed that when Kobe earthquake was applied in the longitudinal direction of the bridge, the lateral displacement of the facing walls of two abutments of the bridge did not follow the same pattern. One of the abutments (on the right side of the bridge, Figure 5-14), moved forward and suffered significant maximum displacement of more than 12 in. (30 cm) which happened at the top of the facing wall and linearly decreased towards the bottom of the abutment. In the abutment on the other side of the bridge the displacement of the facing wall increased with depth and reached a maximum value of 4 in. (10 cm) in the middle height of the wall and decreased towards the bottom of the facing wall.

When Kobe earthquake was applied in the transverse direction of the bridge, the displacement of the facing walls of two abutments of the bridge followed almost the same pattern. In right-side abutment (Figure 5-14) the displacement of the facing wall increased with depth and reached a maximum value of 3 in. (7.5 cm) in the middle height of the wall and decreased towards the bottom of the facing wall. The other abutment, experienced a maximum displacement of 2 in. (5 cm) in the middle height of the wall as shown in Figure 5-18. Similar results were obtained when the model was subjected to the Northridge earthquake in Figures 5-19 and 5-20.

Figures 5-21(a) and 5-21(b) show the deformed geometry of the bridge after being subjected to the Kobe (1995) earthquake motion in the longitudinal direction. Figures 5-22(a) and 5-22(b) show the deformed geometry of the bridge after being subjected to the Kobe (1995) earthquake motion in the transverse direction. As the shown in the figure, the entire bridge abutment system is stable. But some displacements are evident in the facing blocks located on the corners of the GRS abutment. More blocks were slipping when the earthquake applied in transverse direction. The top three rows remained intact since they are tied using rebar and mortar. It can be suggested that the same technique be used for the corner blocks of the wall to provide more stability and prevent the slipping of the facing blocks.

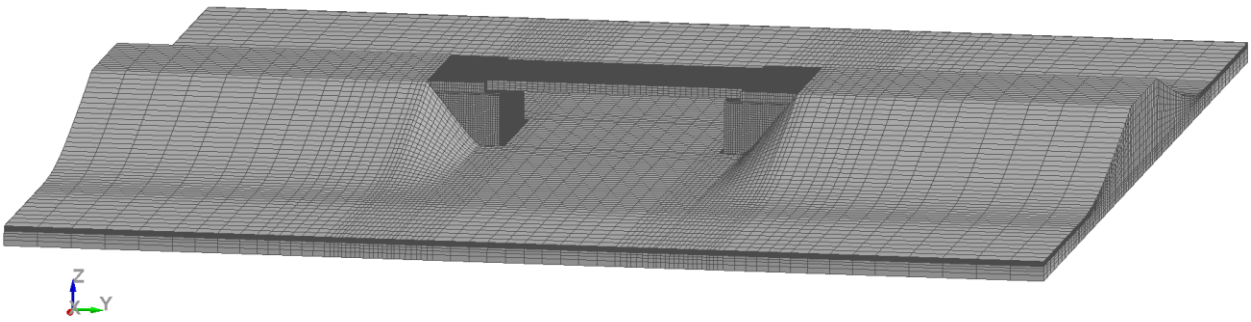

Figure 5-14 Finite Element Model 3D bridge system

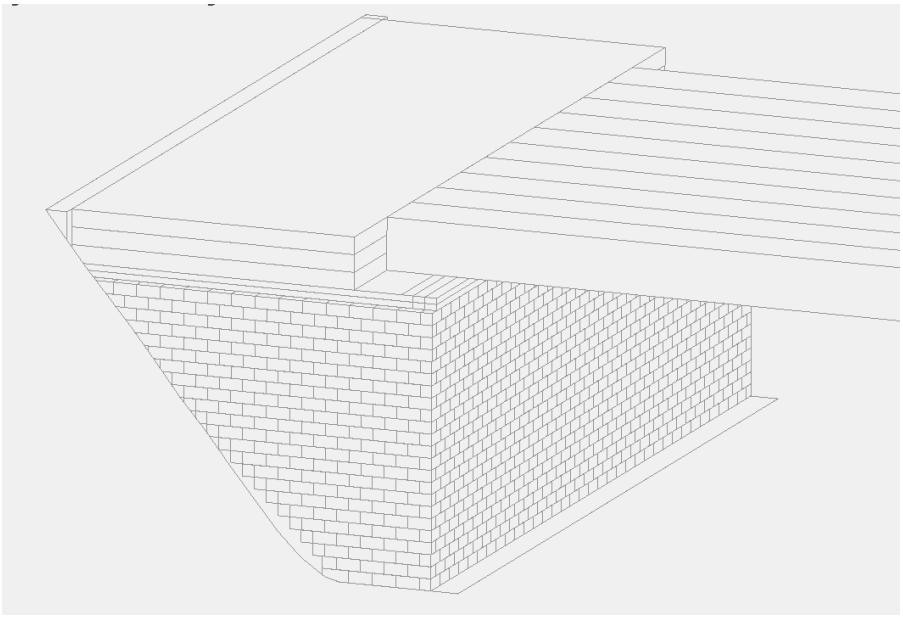

Figure 5-15 GRS bridge abutment of the 3D bridge system

Figure 5-16 Geosynthetic arrangement of the GRS bridge abutment of the 3D bridge system

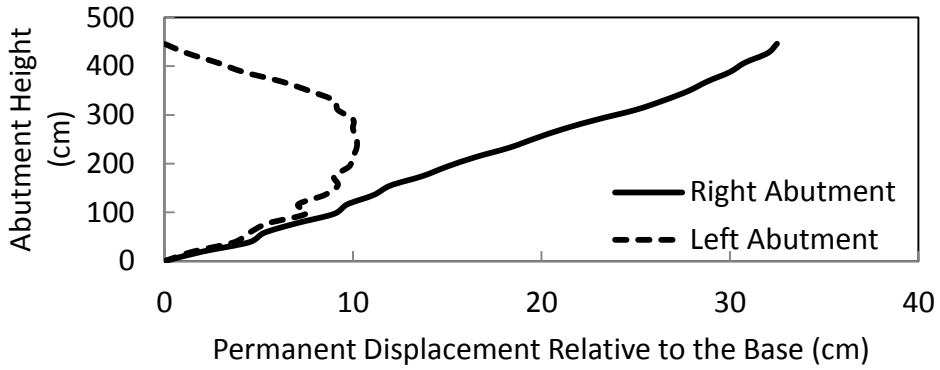

Figure 5-17: Lateral deformation of the abutment when subjected to Kobe earthquake in longitudinal direction

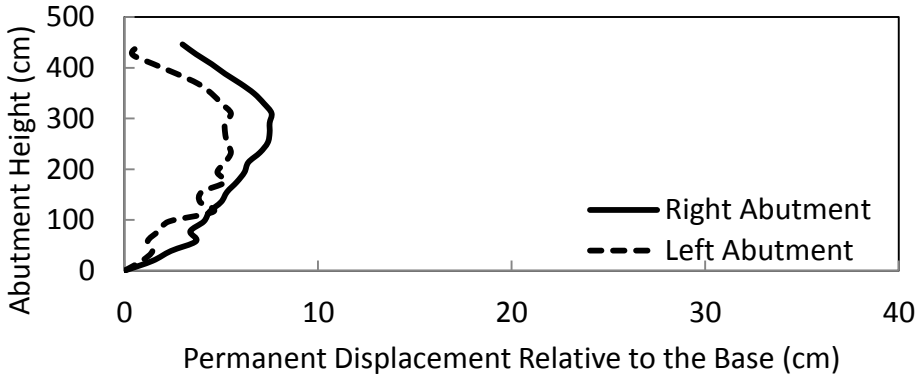

Figure 5-18: Lateral deformation of the abutment when subjected to Kobe earthquake in transverse direction

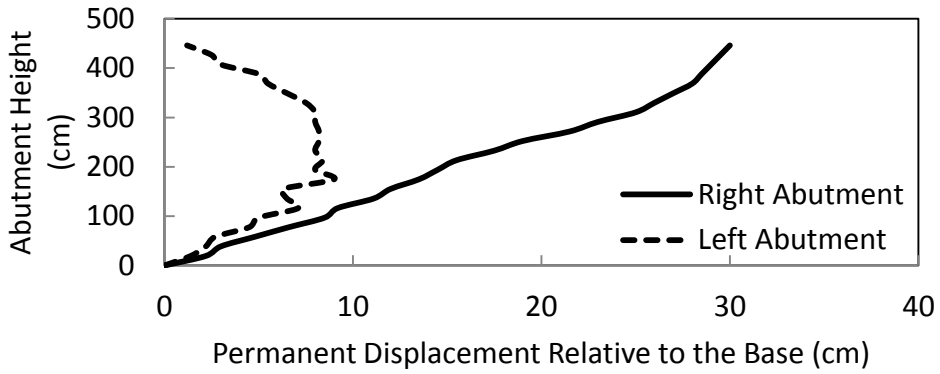

Figure 5-19: Lateral deformation of the abutment when subjected to Northridge earthquake in longitudinal direction

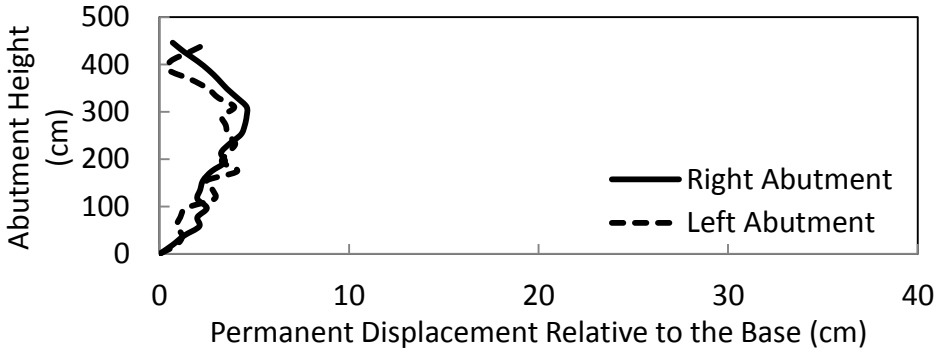

Figure 5-20: Lateral deformation of the abutment when subjected to Northridge earthquake in transverse direction

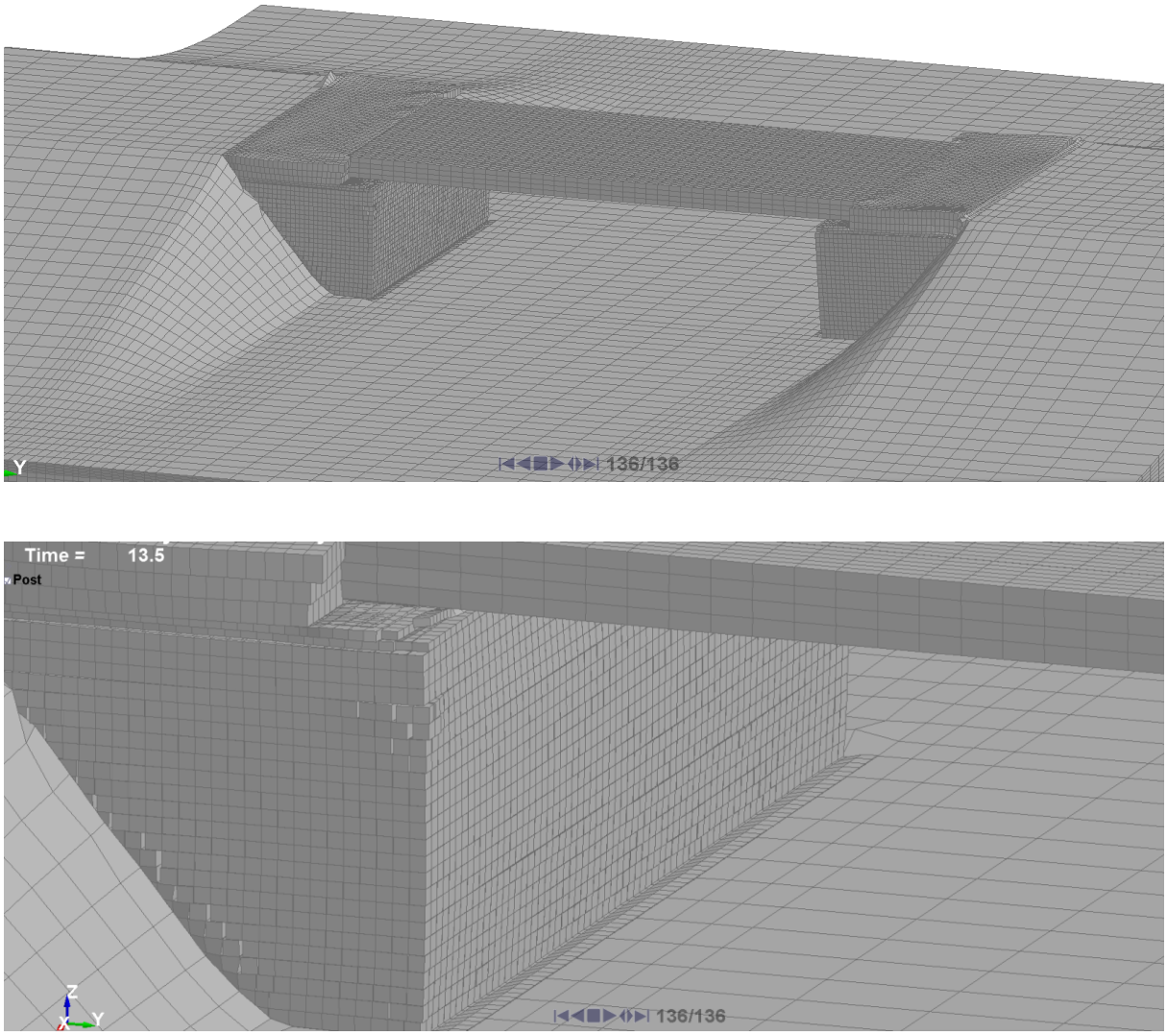

5-21 Deformed geometry of the GRS bridge abutment model after the application of the Kobe (1995) earthquake in the longitudinal direction.

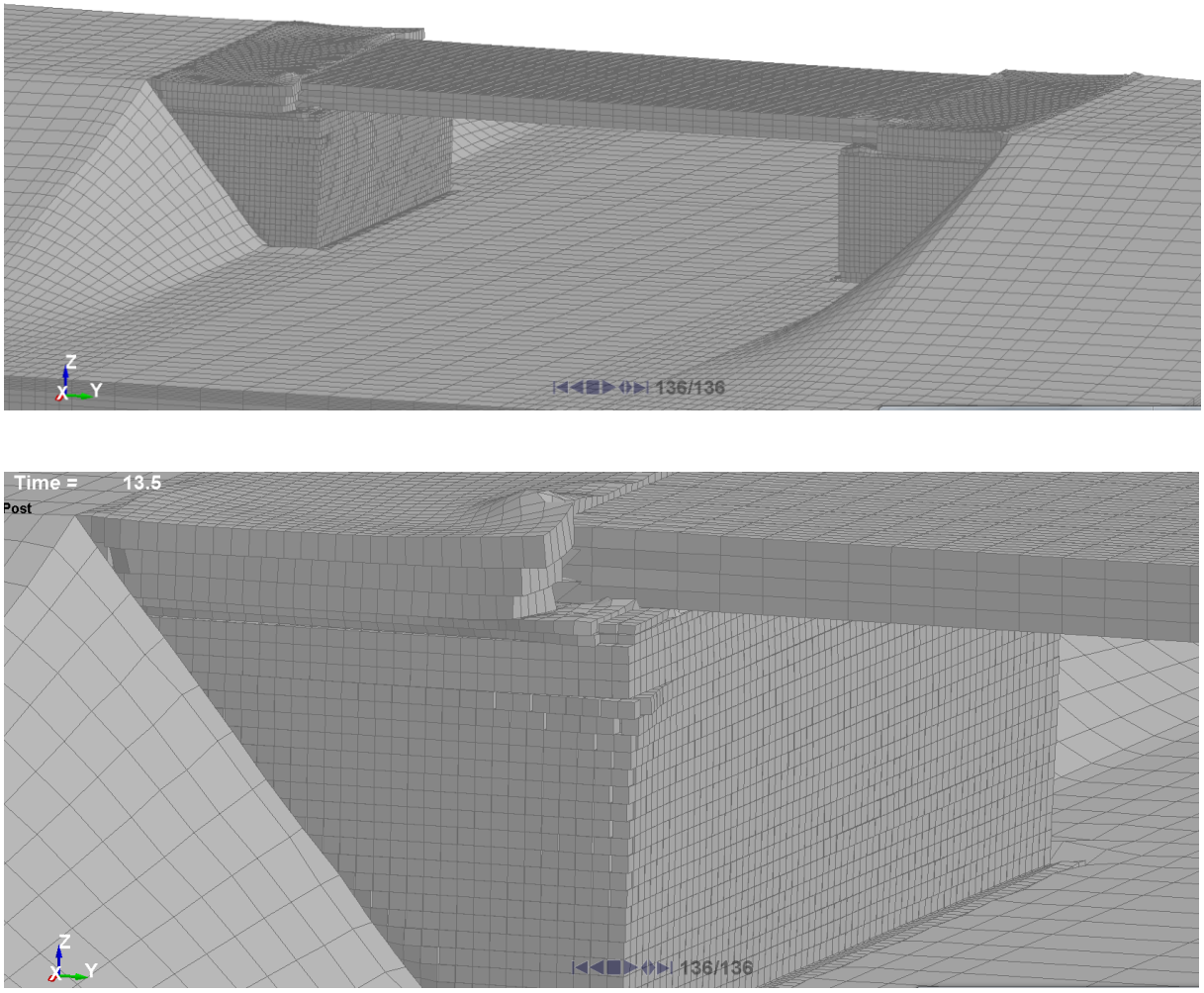

5-22 Deformed geometry of the GRS bridge abutment model after the application of the Kobe (1995) earthquake in the transverse direction.

Chapter 6: SUMMARY AND CONCLUSIONS

This research describes the validation of a finite element model where its analytical results were compared with the results of the instrumented full-scale GRS bridge abutment shake table test. After validation, finite element modeling was used to perform rigorous parametric analyses on the GRS abutments subjected to various earthquake loading.

The GRS abutment test model was designed by following the ASD design method for 0.2 g ground acceleration. The model withstood the vertical and horizontal loads placed on it during ground accelerations of 0.15 g at 1.5 Hz, without experiencing any structural failure or significant movement. The model also safely withstood the unusually large seismic loads while being subjected to ground accelerations up to 1.0 g at 3 Hz. Through testing it became apparent that when properly designed and constructed, GRS bridge abutment is a sensible solution to transfer bridge loads during strong earthquakes. However, the load-carry capacity of a GRS abutment at high ground accelerations may be compromised by sliding of the sill if the bearing pads are not properly designed. Being the only link between the superstructure and the substructure, the bearing pads play a key role in the performance of an abutment. It is suggested that if elastomeric bearing pads are chosen for a GRS bridge abutment that they not only to be designed per AASHTO requirements but also to have a lower natural frequency than the expected high energy frequency range of ground motion anticipated on the construction site (if possible). As seen in testing, if the natural frequency of the bearing pads is below the ground motion's frequency, the horizontal motion of the superstructure can be isolated from the substructure, hence significantly reduces the horizontal forces exerted on the abutment.

The GRS abutment test provided data related to the internal behavior of the abutment during testing, such as accelerations transferred within the model, the envelope of maximum stresses in the geosynthetic reinforcement, and the pressure distribution. The data has shown favorable performance of the GRS abutment-bridge system even when subjected to horizontal accelerations exceeding 1.0 g. While all the components of the design procedures presented in this study cannot be completely validated, it can be concluded, based on the shake table tests results and the results of the parametric study, that GRS abutments have proven to be a strong viable solution for bridge support in seismically-active areas.

The shake table tests have clearly shown that the GRS abutment with realistic bridge loading was able to withstand severe ground shaking in excess of 1.0 g even though the abutment was only designed to withstand a peak ground acceleration of 0.2 g according to the allowable stress design (ASD) method. It is important to note that seismic design of the GRS abutment for the shake table test resulted in an abutment that is of identical configuration to a GRS abutment designed only for static loading following the static design method presented by Wu et al. (2006), with the exception of added bearing pads and expansion joints at the end of the bridge. This reveals that GRS abutments, even being designed for static loads only, are inherently capable of withstanding large ground accelerations. The parametric analysis performed in the present study indicated that GRS abutments can withstand large earthquakes without exerting excessive stresses on the bridge superstructure.

In order to study the effect of earthquake direction (both longitudinal and transverse direction) on GRS bridge abutment system, a three dimensional bridge model was created using LS-DYNA. Two earthquake histories of Kobe 1995 (6.9 Magnitude) and Northridge 1994 (6.7 Magnitude) were considered as input motions. The horizontal component of the earthquake was applied in either the longitudinal direction or transverse direction of the bridge.

The analyses showed that the bridge-abutment system remained stable and the permanent deformations of the GRS abutments were deemed acceptable following destructive earthquakes such as Kobe and Northridge.

References:

1- Abu-Hejleh, N., Wang, T., and Zornberg, J.G. (2000). "Performance of Geosynthetic reinforced Walls Supporting Bridge and Approaching Roadway Structures." *ASCE Geotechnical Special Publication No. 103, Advances in Transportation and Geoenvironmental Systems Using Geosynthetics* , 218–243.

2- Adams, M., Nicks, J., Stabile, T., Wu, J., Schlatter, W. and Hartmann, J. (2011). "Geosynthetic Reinforced Soil Integrated Bridge System, Synthesis Report." *Rep. No. FHWA-HRT-11-027*, Federal Highway Administration, McLean, VA.

3- Bathurst R. J., Cai, Z., Alfaro, M., and Pelletier, M. (1997). "Seismic Design Issues for Geosynthetic Reinforced Segmental Retaining Walls." *Mechanically Stabilized Backfill*, Wu, ed., A. A. Balkema Publishers, Rotterdam, The Netherlands, 79-97.

4- Bathurst, R.J., El-Emman, M.M., and Mashhour, M.M. (2002)."Shaking table model study on the dynamic response of reinforced soil walls." *Proceedings of 7th.international conference on geosynthetis*, Vol. 1, Nice, France, 99-102.

5- Chen, W.F. and Baladi, G. Y. (1985). "Soil Plasticity, Theory and Implementation." *Elsevier Science Publication Co.*, N.Y..

6- Desai, C.S. and Siriwardane, H.J., (1984). "Constitutive Laws for Engineering Materials with emphasis on Geological Materials." *Prentice Hall*.

7- DiMaggio, F.L. and Sandler, I.S. (1971). "Material model for granular soils." *J. Engrg. Mech. Div.*, ASCE, 97(3) 935-950.

8- Duncan, J.M., Byrne, P.M., Wong, K.S. and Mabry, P. (1980). "Strength, Stress-Strain and Bulk Modulus Parameters for Finite Element Analyses of Stresses and Movements in Soil Masses." *Report No. UCB/GT/80-01*, University of California, Berkeley.

9- El-Emam, M., Bathurst, R.J., and Hatami, K. (2004). "Numerical Modeling of Reinforced Soil Retaining Walls Subjected to Base Acceleration." *13th World Conference on Earthquake Engineering*, Vancouver, BC, Canada, Paper No. 2621.

10- Fakharian, K. and Attar, I.H. (2007). "Static and seismic numerical modeling of geosynthetic-reinforced soil segmental bridge abutments." *Geosynthetics International*, Vol. 14, Issue 4, 01, 228 –243.

11- Hatami, K., and Bathurst, R.J. (2000b). "Investigation of Seismic Response of Reinforced Soil Retaining Walls." *4th International Conference on Recent Advances in Geotechnical Earthquake Engineering and Soil Dynamics*, San Diego, CA, USA, Paper No. 7.18.

12- Helwany, S., Budhu, M., and McCallen, D. (2001). "Seismic Analysis of Segmental Retaining Walls–I: Model Verification." *Journal of Geotechnical and Geoenvironmental Engineering*, American Society of Civil Engineers, Vol. 127, No. 9, 741-749.

13- Helwany, S., Wu, J.T.H, and Kitsabunarat, A. (2007). "Simulating the Behavior of GRS Bridge Abutments.", *Journal of Geotechnical and Geoenvironmental Engineering*, American Society of Civil Engineers, Vol. 133, No. 10, 1229-1240.

14- Helwany, S., Wu, J., and Meinholz, P. (2012). "Seismic Design of Geosynthetic-Reinforced Soil Bridge Abutments with Modular Block Facing." *National Cooperative Highway Research Program (NCHRP) WOD 187*.

15- Holtz, R. D., Christopher, B. R., and Berg, R. (1997). "*Geosynthetic Engineering.*" *BiTech Publishers*, Vancouver, Canada.

16- Howard, R.W.A. Jr., Kutter, B.L., and Siddharthan, R. (1998). "Seismic deformation of Reinforced Soil Centrifuge Models." Geotechnical *Earthquake Engineering and Soil Dynamics III*, Dakoulas, P., Yegian, M., and Holtz, B., Ed., ASCE Geo-Institute , Proceedings of a Specialty Conference, Geotechnical Special Publication No. 75, Vol. 1, Seattle, Washington, 446-457.

17- Isenberg, J., Vaughan, D.K. and Sandler, I.S. (1978). "Nonlinear soil structure interaction." *EPRI Report NP-945*, Weidlinger Associates.

18- Keller, G. R. and Devin, S.C. (2003). "Geosynthetic-Reinforced Soil Bridge Abutments." *Transportation Research Record* 1819, Vol. 2, 362–368.

19- Koga, Y., Ito, Y., Washida, S. and Shimazu, T. (1988). "Seismic resistance of reinforced embankment by model shaking table tests.", *International Geotechnical Symposium on Theory and Practice of Earth Reinforcement*, Fukuoka, Japan, 413-418.

20- Koseki, J., Munaf, Y., Tatsuoka, F., Tateyama, M., Kojima, K., and Sato, T. (1998). "Shaking and tilt table tests of geosynthetic-reinforced soil and conventional-type retaining walls." *Geosynthetics International*, 5(1-2), 73-96.

21- Krishna, A.M. and Latha, G.M. (2007). "Seismic response of Wrap-Faced- Reinforced Soil Retaining Wall Models Using Shaking Table Tests." *Geosynthetic International*, Vol. 14, No. 6,. 355-364.

22- Lee, K.Z.Z., Chang, N.Y., and Ko, H.Y. (2010). "Numerical Simulation of Geosynthetic Reinforced Soil Walls Under Seismic Shaking." *Geotextiles and Geomembranes*, 28, 317-334.

23- Ling, H.I., Liu, H., Kaliakin, V., and Leshchinsky, D. (2004). "Analyzing dynamic behavior of geosynthetic-reinforced soil retaining walls." *Journal of Engineering Mechanics*, ASCE, 130(8), 911-920.

24- Ling, H.I., Mohri, Y., Leshchinsky, D., Burke, C., Matsushima, K., and Liu, H. (2005). "Large-Scale Shaking Table Tests on Modular-Block Reinforced Soil Retaining Walls.", *Journal of Geotechnical and Geoenvironmental Engineering*, Vol. 131, No. 4, 465-476.

25- Liu, H., Wang, X., and Song, E. (2010). "Centrifuge testing of segmental geosyntheticreinforced soil retaining walls subjected to modest seismic loading." *Advanced in Analysis, Modeling & Design*, Florida, USA, 2992-2998.

26- Liu, H., Wang, X., Song, E. (2011). "Reinforcement load and deformation mode of geosynthetic-reinforced soil walls subject to seismic loading during service life." *Geotextiles and Geomembranes*, Vol.29, No.1, 1-16.

27- LS-DYNA (2006). "Theory Manual." *Livermore Software Technology Corporation*, Livermore, CA, U.S.A.

28- Mannsbart, G. and Kropik, O. (1996). "Nonwoven Geotextile Used for Temporary Reinforcement of a Retaining Structure under a Railroad Track." *Geosynthetics: Applications, Design and Construction* , DeGroot, Hoedt, and Termaat, ed., A. A. Balkema Publishers, Rotterdam, The Netherlands, 121–124.

29- Matsuo, O., Tsutsumi, T., Yokoyama, K. and Saito, Y. (1998). "Shaking table tests and analyses of geosynthetic-reinforced soil retaining walls." *Geosynthetics International*, Vol.5, I1-2; 97-126.

30- Murata, O., Tateyama, M. and Tatsuoka, F.(1994). "Shaking table tests on a large geosynthetic-reinforced soil retaining wall model." *Recent case histories of permanent geosynthetic-Reinforced soil retaining walls*, tatsuoka & leshchinsky, ed., Balkema, Rotterdam, ISBN 9054103582.

31- Nova-Roessing, L. and Sitar, N. (1998). "Centrifuge Studies of the Seismic Response of Reinforced Soil Slopes." *Geotechnical Earthquake Engineering and Soil Dynamics III*,

Dakoulas, P., Yegian, M., and Holtz, B., Ed., ASCE Geo-Institute, Proceedings of a Specialty Conference, Geotechnical Special Publication No. 75, Vol. 1, Seattle, Washington, 458-468.

32- Perez, A. and Holtz, R. (2004). "Seismic Response of Reinforced Steep Soil Slopes: Results of a Shaking Table Study." *Proc., Geo-Trans 2004, Geotech. Engrg. for Transportation Projects*, Mishac, K.Y. and Edward, K. Eds, ASCE, GSP 126, L. A., CA, USA, 1664-*1672*.

33- Sakaguchi, M. (1996). "A Study of the Seismic Behavior of Geosynthetic Reinforced Walls in Japan." *Geosynthetics Int.*, 3(1), 13-30.

34- Ramakrishnan, S., Budhu, M., and Britto, A. (1998). "Laboratory Seismic Tests on Geotextile Wrap-faced and Geotextile-reinforced Segmental Retaining Walls." *Geosynthetics Int.*, 5(1-2), 55-71.

35- Richardson, G.N., Feger, D., Fong, A., and Lee, K.L. (1977). "Seismic testing of reinforced earth walls." *Journal of Geotechnical Engineering Division*, 103(1), 1–17.

36- Richardson, G.N., and Lee, K.L. (1975). "Seismic design of reinforced earth walls." *Journal of Geotechnical Engineering Division*, 101(2), 167–188.

37- Sabermahani, M., Ghalandarzadeh, A., Fakher, A. (2009). "Experimental study on seismic deformation modes of reinforced-soil walls." *Geotextiles and Geomembranes*, Vol. 27, Issue 2, 121-136.

38- Sakaguchi, M. (1996). "A Study of the Seismic Behavior of Geosynthetic Reinforced Walls in Japan.", *Geosynthetics International*, Vol.3, No. 1, 13-30.

39- Sugimoto, M., Ogawa, S., and Moriyama, M. (1994). "Dynamic Characteristics of Reinforced Embankments with Steep Slope by Shaking Model Tests." *Recent case histories of*

Permanent Geosynthetic-Reinforced Soil Retaining walls, Tatsuoka, F. and Leshchinsky, D., Ed., Balkema, Proceedings of Seiken Symposium No. 11, Tokyo, Japan, 271-275.

40- Wolfe, W.E., Lee, K.L., Rea, D., and Yourman, A.M. (1978). "The Effect of Vertical Motion on the Seismic Stability of Reinforced Earth walls." *Proc. of Symp. on Earth Reinforcement*, ASCE, Pittsburg, Pennsylvania, 856-879.

41- Won, G.W., Hull, T., and De Ambrosis, L. (1996). "Performance of a Geosynthetic Segmental Block Wall Structure to Support Bridge Abutments." *Earth Reinforcement*, Ochiai, Yasufuku, and Omine, ed., A. A. Balkema Publishers, Rotterdam, The Netherlands, Vol. 1, 543–548.

42- Wu, J.T.H. (1994). "Design and Construction of Low Cost Retaining Walls: The Next Generation in Technology." *Publication No. CTI-UCD-1-94*, Colorado Transportation Institute, Denver, Colorado, USA.

43- Wu, J. T. H., Ketchart, K., and Adams, M. T. (2001). "GRS Bridge Piers and Abutments." *Report FHWA-RD-00-038*, FHWA, U.S. DOT.

44- Wu, J.T.H., Lee, K.Z.Z., Helwany, S.B., and Ketchart, K. (2006). "Design and Construction Guidelines for GRS Bridge Abutment with a Flexible Facing." *NCHPR Rep. No. 556*, National Cooperative Highway Research Program, Washington, DC.

46- Zaman, M. M., Desai, C. S., and Faruque, M. O. (1982). "An Algorithm for Determining Parameters for Cap Model from Raw Laboratory Test Data." *Proc. 4th Int. Conf. Numer. Methods Geomech.*, Vol. 1, Edmonton, Canada, Eisenstein. Z. (Ed.), Balkema Press, Rotterdam, 275-285.

CURRICULUM VITAE

Roonak Ghaderi

Education:

PhD Candidate in Civil Engineering, 2016, Department of Civil Engineering and Mechanics, University of Wisconsin-Milwaukee, USA.
Master of Science. in Civil-Geotechnical Engineering, Isfahan University of Technology, Isfahan, Iran.
Bachelor of Science in Civil Engineering, University of Tabriz, Tabriz, Iran.

Teaching Experiences:

Instructor for:

- **Dynamics,** University of Wisconsin-Fox Valley, Fall 2014.
- **Engineering Fundamentals,** University of Wisconsin-Fox Valley, fall 2014.
- **Strength of Materials**, University of Wisconsin-Fox Valley, Spring 2015.
- **Soil Mechanics and Foundation Engineering,** Azad University of Mahabad, Iran, Jan. 2006-Dec. 2007.
- **Engineering Geology,** Azad University of Mahabad, Iran, Jan. 2006-Dec. 2007.

Teaching Assistant for:

- **Strength of Materials (CE-303),** Department of Civil Engineering, University of Wisconsin-Milwaukee, Sep. 2011-May 2012.
- **Statics (CE-201),** Department of Civil Engineering, University of Wisconsin-Milwaukee, Sep. 2010-May 2011.
- **Soil Mechanics (CE-335),** Department of Civil Engineering, University of Wisconsin-Milwaukee, Wisconsin, Jan. 2010-May 2010.
- **Foundation Engineering (CE-456),** Jan. 2008 – May 2012

Designed and graded exams, course projects and home works.

Research Experiences:

PhD research Topic: Seismic Analysis of Geosynthetic Reinforced Soil (GRS) Bridge Abutments with Modular Block Facing; Advisor : Professor Sam Helwany.

Research Assistant, Department of Civil Engineering, University of Wisconsin-Milwaukee, Wisconsin, Jan. 2008-Dec. 2009. Seismic Analysis of Geosynthetic Reinforced Soil (GRS) Bridge Abutments with Modular Block Facing. Studied the design methods of GRS retaining walls, Designed and Conducted soil lab tests, Conducted 3D Finite Element modeling of a full scale shake table test on bridge abutment using computer program **LSDYNA**.

Research Assistant, Department of Civil Engineering, University of Wisconsin-Milwaukee, Wisconsin, Jun. 2009-Aug. 2009. Prepared a step by step example based instruction manual for the new users to the **ABAQUS**, a finite element software used in engineering modeling.

M.Sc. research Topic: Stability Analysis of Geosynthetic Reinforced Slopes via Finite Element Method; Advisor: Professor Mahmood Vafaeian. Conducted finite element modeling of Geosynthetic reinforced slopes using **PLAXIS** software.

Working Experiences:

Project Engineer, Daryakhakpay Consulting Engineers, Tehran, Iran, June 2004-Sep.2007. Conducted Geotechnical studies including site evaluation and ordering required lab and field soil testing, analyzing test results and defining soil profile and soil characteristics, designing Foundations and piles and preparing Geotechnical reports.

Project Engineer; Ghods Niroo Consulting Engineers, Tehran, Iran, Dec. 2003- June 2004. Conducted borrow material study for earth dams including site evaluation, determining the required lab and field soil testing and analyzing the results and preparing reports.

Coordinator, Quantity Surveyor; Saze Gostar Sepahan Contractor Company, Isfahan, Iran, Sep. 2002- July 2003.
Coordinator and quantity .surveyor for a project of a 9-story residential building

Computer skills

LSDYNA, ABAQUS, ANSYS, PLAXIS, SLOPEW, SAP, ETABS, LPILE and Microsoft Office (Excel, Word, PowerPoint).

Publications:

"CLSM Bridge Abutments - Finite Element Modeling and Parametric Study. " V. Alizadeh, S. Helwany, A. Ghorbanpour, M. Oliva, R. Ghaderi, *Computers and Geotechnics*, 64, 61-71, 2015.

"Seismic Behavior of Geosynthetic-Reinforced Soil Bridge Abutments-Experimental Study." Sam Helwany, Jonathan Wu, Philip Meinholz and Roonak Ghaderi. Transportation Infrastructure Geotechnology Journal (Accepted).

"Seismic Behavior of Geosynthetic-Reinforced Soil Bridge Abutments-Analytical Study." Roonak Ghaderi, Sam Helwany, Jonathan Wu, Philip Meinholz and Vahid Alizadeh. Transportation Infrastructure Geotechnology Journal (Accepted).

R. Qhaderi, M. Vafaeian, H. Hashemolhoseini, "A Parametric Study of the Behavior of Geosynthetic Reinforced Soil Slopes"; *Int. J. of Eng., Vol. 18, No4, Nov. 2005*.